

MULTISTABLE SYNCHRONOUS POWER FLOWS: FROM GEOMETRY TO ANALYSIS AND COMPUTATION*

SABER JAFARPOUR[†], ELIZABETH Y. HUANG[†], KEVIN D. SMITH[†], AND
FRANCESCO BULLO[†].

Abstract. The phenomenon of multistability, in which systems have multiple stable operating points, is central to power grid operations like optimal power flow and transient stability. Transitions between stable states may create undesirable circulating flows and lead to inefficiencies and blackouts. Unfortunately, it is not yet fully understood how many stable states exist, how to characterize them, and how to compute them efficiently. A deeper understanding of multistability, including its dependence upon network structures and power transmission, may lead to more reliable and efficient power flows in future grids.

This paper provides a rigorous and comprehensive framework for studying the multistability of active power flows in lossless grids. This problem is equivalent to both the equilibrium analysis of the coupled swing equations and the synchronization problem for Kuramoto oscillators. The proposed framework is based on a novel *winding partition* of the n -torus into winding cells, defined by *Kirchhoff's angle law* for undirected graphs. The winding partition possesses several useful properties, including notably that each winding cell contains at most one equilibrium power flow solution. This paper also proposes a complete algorithm to compute these equilibrium points using a novel contraction mapping. Finally, we apply our results to numerically study multistability in several test cases and estimate power capacity and congestion.

Key words. Multistability, power networks, graph theory, Kuramoto oscillators, cycle structure of a graph

AMS subject classifications. 37C25, 93C10, 37C75, 37C65, 37N35

1. Introduction.

Problem description and motivation. Power grids are among the most complex and important societal infrastructures, responsible for efficiently and reliably transmitting power from generators to customers. One operational challenge endemic to the power grid is that patterns of power flow change over time. As distributed energy resources take on a greater share of power demand, for example, the spatial distribution of generation changes—resulting in new pattern of power flows in transmission lines. A key problem, therefore, is to develop physically insightful, mathematically rigorous, and computationally efficient techniques to study power flows and understand their effects on power system stability.

An important feature in stability analysis of power grids is the existence of multistable synchronous flows in the network. Even with a fixed set of power injections and a fixed topology, the active power flow equation can admit several solutions, corresponding to several stable operating points. Multistability introduces a problem of hysteresis: if a disturbance moves the system state to a less-desirable equilibrium, then returning the system to its nominal state may be more difficult than eliminating the disturbance. It is well-known that the transition between these distinct stable operating points is usually accompanied by undesirable large changes in the circulating

*This work was supported in part by the Solar Energy Technologies Office of the U.S. Department of Energy under Contract No. DE-EE0000-1583 and by the Defense Threat Reduction Agency under Contract No. HDTRA1-19-1-0017. Figures 2, 3, 4, 5, 6, 7, and 11 are licensed under Creative Commons Attribution-ShareAlike 4.0 International License (CC BY-SA 4.0) and are reproduced with permission from [7].

[†]Center for Control, Dynamical Systems, and Computation, Departments of Mechanical Engineering and of Electrical and Computer Engineering, University of California, Santa Barbara (saber, eyhuang, kevinsmith, bullo@ucsb.edu).

power flows.

Circulating flows (also known as loop flows) are power flows around cycles in the network and are particularly interesting from the perspective of power grid stability. Circulating flows are regarded as both a blessing and a curse to power transmission. In some cases, they are undesirable—circulating flows do not deliver usable power to customers, but they have the potential to increase power losses, threaten the system’s stability and security by increasing line congestion, and cause pricing volatility. However, in other cases, circulating flows actually increase the transmission capacity of a network along certain pathways. The Lake Erie loop, which consists of roughly 1000 miles of transmission lines through Ontario and five American states, is a classic example of the challenge that circulating flows present to power grid stability [19]. For instance, the 2003 US Northeast blackout began with a unpredictable and volatile shift in the direction of the flow around the Lake Erie loop. As a second example, starting in 2008, volatility and unexpected changes in the direction and magnitude of loop flows around the lake were observed [45]; these phenomena increased the west-to-east transmission congestion and the wholesale electricity costs in the New York area.

Several causes of circulant flows have been identified, all of which are related to shifts in the system’s stable operating points. In some cases, changes in the distribution of power injections (and withdrawals) across the network cause the stable operating point to change, corresponding to a change in circulant flows. In other cases, loop flows result from changes in network topology—either when a line trips, destroying a cycle; or when a previously open line is closed, creating a new cycle [9]. Changes to topology, of course, result in changes to the system’s stable operating points. Whether caused by changes in power injections or topology, circulant flows emerge when the system’s stable operating point suffers a relocation. Therefore, in order to understand circulant flows, it is critical to characterize their emergence as a function of equilibrium power flows and, in turn, of power injections and topology.

The historical precedence for circulant flows causing catastrophic system failure, as well as their paradoxical nature as both a hindrance and a boon to power transmission, motivate a theoretical understanding of different operating points of the system and their loop flows. In particular, for analysis and design purposes, it is crucial for power system operators to have rigorous answers to the following fundamental questions about active power flow:

- Q_1 : how many stable operating points do there exist for a power grid?
- Q_2 : can the operating points be distinguished, characterized and localized?
- Q_3 : can a complete algorithm compute each equilibrium point in polynomial time and with convergence guarantees?
- Q_4 : what are the properties of the circulating power flows associated to the various operating points?
- Q_5 : what is the network power transmission capacity and how does it relate to the operating points?

Literature review. The power flow equations [26] describe the steady-state flow of active and reactive power in AC power and grids, are universal in power systems engineering. Modeling the dynamics of power systems *away* from steady state, perhaps for the purpose of transient stability analysis, is much more challenging. Two of the simplest dynamic models are the second-order coupled swing equations [5, 3], and their first-order variant, the Kuramoto model [2, 4, 12, 41]. These models describes voltage angle dynamics in a grid with constant voltage magnitudes and purely inductive transmission lines. For these two models, the equilibrium condition is equivalent to

the active power flow equation. This equivalence is widely understood and exploited in the literature on synchronization, multistability, and computational methods for the active power flow equations and the Kuramoto model.

Much effort has focused on the study multistable flows in complex networks. Both the physics and power systems communities have examined this problem, with physicists studying the stable equilibrium points for the Kuramoto model, and power systems engineers studying as the multiplicity of solutions to active power flow equations. To our knowledge, [15] is the first paper that studies the multistability in a network of oscillators with ring topology. An algorithm to compute all multistable equilibrium points in a ring network of coupled oscillator is proposed by [43]. The region of attraction of multistable equilibrium points on a k -nearest neighbor graphs is studied in [48]. Related works include the study of multistability in the generalized Kuramoto model in small world graph [32] and in Cayley graphs [34]. In the power network community, [25] is the first paper to rigorously study multistability and establish that the active power flow equations have multistable solutions on a 6-node cycle network with balanced power injections. Several papers [9, 10, 23] have investigated mechanisms that create large loop flows and have shown that loop flows will persist even when the network returns to its normal operating condition. In [9], the basins of attraction for loop flows has been studied using Lyapunov theory. The papers [9, 10, 23] acknowledge the connection between loop flows and winding numbers of the cycles in the graph. In [31], the notion of winding vector for an arbitrary graph is introduced as the sum of the phase differences along a cycle basis. Moreover, it is shown that for a planar graph, there is a one-to-one correspondence between the winding vectors and the equilibrium points of the Kuramoto model with phase differences less than $\pi/2$ [31, Lemma 3]. Finally, by identifying the equilibrium points of the Kuramoto model with the lattice points in a suitable set, an asymptotic estimate on the number of equilibrium points of the Kuramoto model is proposed in [16].

In the literature, many numerical algorithms have been developed to compute exactly and approximately the equilibrium points of the Kuramoto model, i.e., solutions of the active power flow equations. In [35], a numerical method based on parameter homotopy is developed, which is guaranteed to find all the solutions of Kuramoto model. However, the computational complexity of this method is high, and results are reported only for graphs with up to 18 nodes. In [31], a high-level algorithm is proposed for planar networks: by assuming uniform coupling, the paper obtains upper and lower bounds on the number of solutions for ring networks and planar topology. The Holomorphic Embedding Load-Flow Method (HELM) is proposed in [46] to find all solutions of power flow equations. Although HELM is guaranteed to find the operable solution of the power flow equations, it is reported to be much slower than the Newton–Raphson methods [42]. In [30], an algorithm based on a topological continuation argument is developed to solve the power flow problem. However, a counterexample for this method using a five-bus system has been constructed in [38]. This continuation method is revisited and modified in [28]. Techniques for solving the optimal power flow problem (OPF) can also be used to solve the power flow problem. OPF problems have been studied extensively in the power network literature, e.g., see [39, 40, 37]. Unfortunately, due to the non-convex nature of the OPFs, these algorithms are not guaranteed to compute feasible solutions for arbitrary topologies [29].

Contributions. This paper provides a rigorous graph-theoretic and geometric framework for the analysis of the active power flow equations. Our framework answers in comprehensive detail questions (Q_2) – (Q_4) and provides novel insight into

questions (Q₁) and (Q₅). Specifically, this paper makes the following three main contributions:

- (i) we present a novel partition of the n -torus, called the *winding partition*, defined by an undirected graph with cycles; this partition decomposes the n -torus into the union of winding cells;
- (ii) we prove that each winding cell contains at most a unique solution of the active power flow problem, that is, a unique synchronous equilibrium for the Kuramoto model,
- (iii) we present a complete solver for the active power flow problem in the phase-cohesive set, i.e., an algorithm that computes all stable solutions to the active power flow equations (or determines that none exists).

We next discuss these contributions in detail. In Section 2, we provide a novel algebraic graph theory on the n -torus. We establish a fundamental property of angle differences around cycles in graphs, which amounts to a *Kirchhoff's angle law*, generalization of the classic voltage law. We then introduce the notion of winding vector as a function on the n -torus and show that this function takes discrete values. This function therefore implicitly gives rise to a partition of the n -torus into *winding cells*.

In Section 3, we introduce the active power flow problem and the phase-cohesive subset of the n -torus, where phase differences are smaller than $\pi/2$. Using the monotonicity of the active power flow equations on the phase-cohesive sets, we show that in each winding cell there exists at most one stable solution for the active power flow equations. This at-most uniqueness result shows that winding cells can be used to localize the stable solutions of the active power flow equations, thereby providing a graph-theoretic geometric answer to the localization question (Q₂). This result also shows how the winding partition is a key geometric object to study the active power flow problem.

An upper bound on the number of winding cells leads immediately to an upper bound on the number of stable operating points, as asked in (Q₁). In the literature, there are several partial results proving uniqueness of solutions of active power flow equations in certain regions and for special graphs; e.g., see [31, Lemma 3] for planar graphs. Our at-most uniqueness theorem generalizes these results to a partition of the n -torus and to networks with arbitrary topology. The rest of Section 3 is devoted to characterizing the properties of the circulating flows at the operating points of the network, that is, question (Q₄). We show that there is one-to-one correspondence between the winding vector of an operating point and its associated circulating flow. In particular we show that, for a network with a single cycle, the circulating flow increases monotonically with respect to the winding number.

In Section 4, we recast the active power flow equation into a useful novel system of equations with an explicit dependence on the winding vector of the solution. Unlike the active power flow equations, this new formulation, called the *edge balance equations*, has at most one solution. We exploit the edge balance equations and propose an iterative algorithm, called the *projection iteration*, that computes the solution of the active power flow equations in each phase-cohesive winding cell or determines that one does not exist. Using the winding partition and the projection iteration, we propose a complete solver for the active power flow equations in the phase-cohesive set, i.e., an algorithm that is guaranteed to compute all stable solutions to the active power flow equations, as stated in question (Q₃). As we mention above, the literature contains several algorithms for solving the active power flow equations. However, for most of these algorithms, the convergence is guaranteed only for some special topologies. Comparing to the only other complete power flow solver in the literature [35],

our algorithm allows for the treatment of large dimensional systems in a physically meaningful and geometrically intuitive manner.

Finally, in Section 5, we present results from various numerical experiments. We consider three different test cases: 1) a 12-node ring 2) a 12-node line 3) the IEEE RTS 24 testcase. First, we introduce a notion of transmission capacity and a notion of network congestion. We then utilize the projection iteration to numerically study the capacity and congestion in a 12-node ring power grid under two different power profile. Our numerical analysis shows that, for the asymmetric power profile, an increase in loop flow can lead to an increase in the network power capacity. For the IEEE RTS 24 testcase, we design a linear program to find the power profile with large circulating flows in the network. Finally, we compare the time efficiency of the projection iteration versus the Newton–Raphson method for identifying the circulating flow in the network. The numerical analysis in this section shed some light on question (Q₅). However, a comprehensive answer to this question is still far from complete and will be the subject of future research.

1.1. Notation and preliminary concepts. Let \mathbb{R} and \mathbb{C} denote the set of real and complex numbers, respectively. For every $x \in \mathbb{R}^m$ and every $r > 0$, we define the open disk $D_\infty(\mathbf{x}, r)$ by

$$D_\infty(\mathbf{x}, r) = \{\mathbf{y} \in \mathbb{R}^m \mid \|\mathbf{y} - \mathbf{x}\|_\infty < r\}.$$

Algebraic graph theory. Let G denote an undirected graph with nodes $\{1, \dots, n\}$ and edge set \mathcal{E} with cardinality m . Given an arbitrary orientation and ordering of the edges, let B denote the corresponding incidence matrix. If $x \in \mathbb{R}^n$ (with x_i associated to the i th node), then the flow vector associated to x is $B^\top x \in \mathbb{R}^m$ (with $(B^\top x)_e = x_i - x_j$ associated to the oriented edge $e = (i, j)$). A cycle in G is an ordered sequence of three or more nodes such that there is an edge between every two consecutive nodes, the first and last nodes are the same, no other node is repeated. An undirected graph G is *cyclic* if it contains at least one cycle. For a cycle σ in G , the *signed cycle vector* $v_\sigma \in \{-1, 0, 1\}^m$ is defined by

$$(v_\sigma)_e = \begin{cases} +1, & \text{if the edge } e \text{ is traversed positively by } \gamma, \\ -1, & \text{if the edge } e \text{ is traversed negatively by } \gamma, \\ 0, & \text{otherwise.} \end{cases}$$

One can show that $\text{Ker}(B)$, called the *cycle space* of G , is the subspace of \mathbb{R}^m spanned by the signed cycle vectors of all cycles of G . A set $\Sigma = \{\sigma_1, \dots, \sigma_{m-n+1}\}$ is a *cycle basis* for G if the corresponding set $\{v_{\sigma_1}, \dots, v_{\sigma_{m-n+1}}\}$ is a basis for $\text{Ker}(B)$. Given a connected undirected graph G with cycle basis $\Sigma = \{\sigma_1, \dots, \sigma_{m-n+1}\}$, the *cycle-edge matrix* is

$$(1.1) \quad C_\Sigma = \begin{bmatrix} v_{\sigma_1}^\top \\ \vdots \\ v_{\sigma_{m-n+1}}^\top \end{bmatrix} \in \mathbb{R}^{(m-n+1) \times m}.$$

Figure 1.1 shows some polygonal graphs with oriented edges and cycle bases.

Next, assume each edge (i, j) has a weight a_{ij} and define the diagonal edge weight matrix $\mathcal{A} = \text{diag}(a_{ij}) \in \mathbb{R}^{m \times m}$. The Laplacian matrix of G is $L = BAB^\top$. Recall that L is singular and its Moore–Penrose pseudoinverse L^\dagger has the following properties: $LL^\dagger L = L$, $L^\dagger LL^\dagger = L^\dagger$, $L^\dagger L = (L^\dagger L)^\top$, and $LL^\dagger = (LL^\dagger)^\top$. The *cutset projection*

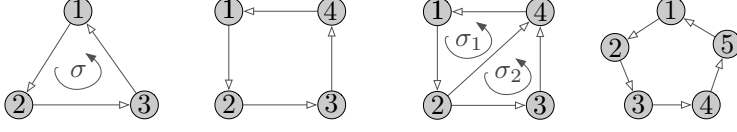


Fig. 1.1: The triangle, the square, the square-with-diagonal, and the pentagon graph. The triangle and the square-with-diagonal graphs are drawn with a cycle basis.

matrix \mathcal{P}_{cut} is the oblique projection onto $\text{Img}(B^\top)$ parallel to $\text{Ker}(BA)$ given by

$$\mathcal{P}_{\text{cut}} = B^\top L^\dagger BA.$$

The weighted cutset projection matrix \mathcal{P}_{cut} is idempotent, and 0 and 1 are eigenvalues with algebraic (and geometric) multiplicity $m-n+1$ and $n-1$, respectively. Additional properties of \mathcal{P}_{cut} are in [22, Theorem 5]. Similarly, the *cycle projection matrix* \mathcal{P}_{cyc} is the oblique projection onto $\text{Ker}(BA)$ parallel to $\text{Img}(B^\top)$ given by

$$\mathcal{P}_{\text{cyc}} = I_m - B^\top L^\dagger BA.$$

The n -torus. Given angles $\alpha, \beta \in \mathbb{S}^1$, the geodesic distance between α and β , denoted by $|\alpha - \beta|$, is the length of the shortest arc in \mathbb{S}^1 connecting α to β . The *counterclockwise difference* on \mathbb{S}^1 is the map $d_{\text{cc}} : \mathbb{S}^1 \times \mathbb{S}^1 \rightarrow [-\pi, \pi)$ defined by:

$$d_{\text{cc}}(\alpha, \beta) = \begin{cases} |\alpha - \beta|, & \text{if the counterclockwise arc from } \alpha \text{ to } \beta \text{ is shorter than } \pi, \\ -|\alpha - \beta|, & \text{otherwise.} \end{cases}$$

If we identify $\mathbb{S}^1 \simeq [0, 2\pi)$, for every $\alpha, \beta \in [0, 2\pi)$, the counterclockwise difference $d_{\text{cc}}(\alpha, \beta)$ is given by $d_{\text{cc}}(\alpha, \beta) = \text{mod}((\beta - \alpha), 2\pi) - \pi$. Given an undirected graph G with edge orientation and ordering, the *counterclockwise edge difference* $d_G : \mathbb{T}^n \rightarrow [-\pi, \pi)^m$ is defined by

$$(d_G(\theta))_e = d_{\text{cc}}(\theta_i, \theta_j),$$

for each oriented edge $e = (i, j)$. The *punctured n -torus* \mathbb{T}_0^n is

$$\mathbb{T}_0^n = \{\theta \in \mathbb{T}^n \mid |\theta_i - \theta_j| < \pi \text{ for each } (i, j) \text{ edge of } G\}.$$

Note that $\text{closure}(\mathbb{T}_0^n) = \mathbb{T}^n$. One can see that d_G is a continuous function on \mathbb{T}_0^n .

We also need the notion of quotient space. For every angle $s \in \mathbb{S}^1 \simeq [0, 2\pi)$, define the rotation operator $\text{rot}_s : \mathbb{T}^n \rightarrow \mathbb{T}^n$ by $\text{rot}_s(\theta) = (\theta_1 + s, \dots, \theta_n + s)^\top$. Using this rotation operator as a group action, we define the *reduced n -torus* as the quotient space $\mathbb{T}^n / \mathbb{S}^1$ and the *reduced punctured n -torus* as the quotient space $\mathbb{T}_0^n / \mathbb{S}^1$.

2. The winding partition of the n -torus and its properties. In this section, we generalize certain concepts from algebraic graph theory to the setting where the graph nodal variables take value on the torus \mathbb{T} instead of the standard real space \mathbb{R} . We aim to generalize the classic Kirchhoff's voltage law (KVL) to this setting and to study an appropriately defined partition of \mathbb{T}^n .

DEFINITION 2.1 (Winding number, vector, and map). *Let G be a cyclic connected undirected graph and $\theta \in \mathbb{T}_0^n$. Then*

(i) for every cycle σ in G with n_σ nodes, the winding number of θ along σ is

$$w_\sigma(\theta) = \frac{1}{2\pi} \sum_{i=1}^{n_\sigma} d_{cc}(\theta_i, \theta_{i+1}),$$

where we assume $\sigma = (1, \dots, n_\sigma, 1)$ without loss of generality and $\theta_{n_\sigma+1} = \theta_1$ by convention; and

(ii) for every cycle basis $\Sigma = \{\sigma_1, \dots, \sigma_{m-n+1}\}$ in G , the winding vector of θ along the basis Σ is the vector

$$[w_{\sigma_1}(\theta), \dots, w_{\sigma_{m-n+1}}(\theta)]^\top,$$

(iii) for every cycle basis $\Sigma = \{\sigma_1, \dots, \sigma_{m-n+1}\}$ in G , the winding map $\mathbf{w}_\Sigma : \mathbb{T}_0^n \rightarrow \mathbb{Z}^{m-n+1}$ along the basis Σ is

$$\mathbf{w}_\Sigma(\theta) = [w_{\sigma_1}(\theta), \dots, w_{\sigma_{m-n+1}}(\theta)]^\top.$$

Now we study the winding number for the triangle graph with cycle $\sigma = (1, 2, 3, 1)$; see Figure 1.1. Since the cycle space of the triangle graph is spanned by σ , the winding map with respect to σ is $\mathbf{w}_\Sigma(\theta) = w_\sigma(\theta)$. One can show that, if the angles $(\theta_1, \theta_2, \theta_3) \in \mathbb{T}_0^3$ are contained in an arc of length less than or equal to π , then $w_\sigma(\theta) = 0$ and, otherwise, $w_\sigma(\theta) = \pm 1$; see Figure 2.1. For example, for $\phi = (0, \frac{\pi}{3}, \frac{2\pi}{3})^\top$ and

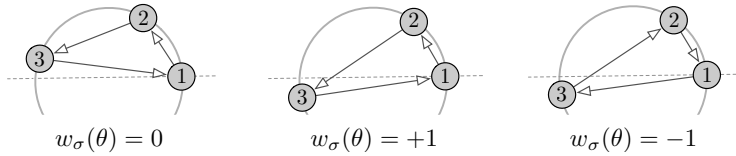


Fig. 2.1: For the triangle graph, if the angles are strictly contained in a half circle, the winding number is zero. Otherwise, the winding number is ± 1 depending upon the node numbering and edge orientations.

$\psi = (0, \frac{2\pi}{3}, \frac{4\pi}{3})^\top$, simple book-keeping shows

$$w_\sigma(\phi) = \frac{1}{2\pi} (\frac{\pi}{3} + \frac{\pi}{3} - \frac{2\pi}{3}) = 0, \quad \text{and} \quad w_\sigma(\psi) = \frac{1}{2\pi} (\frac{2\pi}{3} + \frac{2\pi}{3} + \frac{2\pi}{3}) = 1.$$

Now, we prove some useful properties for the winding number and winding vectors.

THEOREM 2.2 (Kirchhoff's angle law and properties of winding vector). *Let G be a cyclic connected undirected graph with n nodes, m edges, and $m - n + 1$ independent cycles. Let σ be a cycle on G with n_σ nodes. For $\theta \in \mathbb{T}_0^n$,*

(i) $w_\sigma(\theta)$ is an integer and, for $\gamma(\theta) := \max\{|\theta_i - \theta_j| \mid (i, j) \text{ is an edge of } \sigma\} < \pi$,

$$(2.1) \quad |w_\sigma(\theta)| \leq \left\lfloor \frac{\gamma(\theta)n_\sigma}{2\pi} \right\rfloor \leq \left\lfloor \frac{n_\sigma}{2} \right\rfloor - 1;$$

(ii) $w_\sigma(\theta) = \frac{1}{2\pi} v_\sigma^\top d_G(\theta)$, for any orientation of the edges on G .

We refer to property (i) as the Kirchhoff's angle law. Moreover, for every cycle basis $\Sigma = \{\sigma_1, \dots, \sigma_{m-n+1}\}$ of G ,

(iii) the winding map \mathbf{w}_Σ is piecewise constant, its image $\text{Img}(\mathbf{w}_\Sigma)$ is a finite set, and

$$\text{Img}(\mathbf{w}_\Sigma) \subseteq \left\{ u \in \mathbb{Z}^{m-n+1} \mid |u_i| \leq \lfloor n_{\sigma_i}/2 \rfloor - 1, \text{ for } i \in \{1, \dots, m-n+1\} \right\};$$

(iv) if $\alpha_1 v_{\sigma_1} + \dots + \alpha_{m-n+1} v_{\sigma_{m-n+1}} = v_\sigma$ for some scalars $\alpha_1, \dots, \alpha_{m-n+1} \in \mathbb{R}$, then $w_\sigma(\theta) = \alpha_1 w_{\sigma_1}(\theta) + \dots + \alpha_{m-n+1} w_{\sigma_{m-n+1}}(\theta)$ for any $\theta \in \mathbb{T}_0^n$.

Proof. Regarding part (i), suppose that $\sigma = (1, \dots, n_\sigma)$. Note that, for every $\alpha, \beta \in \mathbb{S}^1$ such that $|\alpha - \beta| \leq \gamma$ we have $|d_{cc}(\alpha, \beta)| \leq \gamma$. Thus

$$|w_\sigma(\theta)| = \frac{1}{2\pi} \left| \sum_{i=1}^{n_\sigma} d_{cc}(\theta_i, \theta_{i+1}) \right| \leq \frac{1}{2\pi} \sum_{i=1}^{n_\sigma} |d_{cc}(\theta_i, \theta_{i+1})| \leq \frac{1}{2\pi} n_\sigma \gamma(\theta).$$

Since $w_\sigma(\theta)$ is an integer, we get $|w_\sigma(\theta)| \leq \left\lfloor \frac{\gamma(\theta) n_\sigma}{2\pi} \right\rfloor$. For the second inequality, note that $|d_{cc}(\alpha, \beta)| < \pi$. Thus

$$\frac{\gamma(\theta) n_\sigma}{2\pi} < \frac{n_\sigma}{2}.$$

This implies that $\left\lfloor \frac{\gamma(\theta) n_\sigma}{2\pi} \right\rfloor < \frac{n_\sigma}{2}$. Since $\left\lfloor \frac{\gamma(\theta) n_\sigma}{2\pi} \right\rfloor$ is an integer, we have $\left\lfloor \frac{\gamma(\theta) n_\sigma}{2\pi} \right\rfloor \leq \left\lfloor \frac{n_\sigma}{2} \right\rfloor - 1$.

Regarding part (ii), by definition, if $\sigma = (1, \dots, n_\sigma, 1)$ is a cycle in G , then

$$w_\sigma(\theta) = \frac{1}{2\pi} \sum_{i=1}^{n_\sigma} d_{cc}(\theta_i, \theta_{i+1}).$$

Note that, for every $i \in \{1, \dots, n_\sigma\}$ since the nodes i and $i+1$ are connected by an edge in G , there exists $e \in \mathcal{E}$ such that either $e = (i, i+1)$ or $e = (i+1, i)$. If we have $e = (i, i+1)$, then

$$d_{cc}(\theta_i, \theta_{i+1}) = -(d_G(\theta))_e = (v_\sigma)_e (d_G(\theta))_e.$$

If we have $e = (i+1, i)$, then

$$d_{cc}(\theta_i, \theta_{i+1}) = +(d_G(\theta))_e = (v_\sigma)_e (d_G(\theta))_e.$$

Therefore, in both case, for $e \in \mathcal{E}$, we get $d_{cc}(\theta_i, \theta_{i+1}) = (v_\sigma)_e (d_G(\theta))_e$. As a result,

$$w_\sigma(\theta) = \frac{1}{2\pi} \sum_{r=1}^{n_\sigma} d_{cc}(\theta_i, \theta_{i+1}) = \frac{1}{2\pi} \sum_{e \in \mathcal{E}} (v_\sigma)_e (d_G(\theta))_e = \frac{1}{2\pi} v_\sigma^\top d_G(\theta).$$

Regarding part (iii), first note that part (i) implies $|w_{\sigma_i}| \leq \left\lfloor \frac{n_\sigma}{2} \right\rfloor - 1$, for every $i \in \{1, \dots, m-n+1\}$. In turn, this implies that

$$\text{Img}(\mathbf{w}_\Sigma) \subseteq \left\{ [u_1, \dots, u_{m-n+1}]^\top \mid u_i \in \mathbb{Z}, |u_i| \leq \left\lfloor \frac{n_{\sigma_i}}{2} \right\rfloor - 1, \text{ for } i \in \{1, \dots, m-n+1\} \right\},$$

and therefore the winding map \mathbf{w}_Σ has a finite range. Moreover, the counterclockwise edge difference map $d_G : \mathbb{T}^n \rightarrow [-\pi, \pi]^m$ is continuous on $\mathbb{T}_0^n \subset \mathbb{T}^n$. Thus $\mathbf{w}_\Sigma : \mathbb{T}_0^n \rightarrow \mathbb{Z}^{m-n+1}$ is a continuous map with a finite range. Therefore, the winding map \mathbf{w}_Σ is piecewise constant and this completes the proof of part (iii).

Regarding part (iv), note that, by part (ii), we have $w_\sigma(\theta) = \frac{1}{2\pi} v_\sigma^\top d_G(\theta)$, for every cycle σ . Therefore, we get

$$w_{\sigma_{r+1}}(\theta) = \frac{1}{2\pi} (\alpha_1 v_{\sigma_1} + \dots + \alpha_r v_{\sigma_r})^\top d_G(\theta) = \alpha_1 w_{\sigma_1}(\theta) + \dots + \alpha_r w_{\sigma_r}(\theta).$$

This concludes the proof of the theorem. \square

- REMARKS 2.3. (i) The winding number, winding vector, and winding map are invariant under the rotation operator rot_s , for $s \in [-\pi, \pi)$, that is, every cycle σ and every $\theta \in \mathbb{T}_0^n$ satisfy $w_\sigma(\theta) = w_\sigma(\text{rot}_s(\theta))$. Therefore the winding number, winding vector, and winding map are well-defined on the reduced punctured n -torus $\mathbb{T}_0^n/\mathbb{S}^1$.
- (ii) The winding vector of θ along the basis Σ collects in one quantity all the information required to compute the winding number of each cycle of the graph.
- (iii) The winding number, vector and map \mathbf{w}_Σ and its image $\text{Img}(\mathbf{w}_\Sigma)$ depend on the cycle basis Σ chosen for G . However, using the linearity property of the winding numbers in Theorem 2.2(iv), one can define a basis-independent winding map on \mathbb{T}_0^n . Let $\text{Ker}'(B)$ be the dual space of the cycle space $\text{Ker}(B)$ and let $\{v'_{\sigma_1}, \dots, v'_{\sigma_{m-n+1}}\}$ be the dual basis on $\text{Ker}'(B)$, associated to the basis $\{v_{\sigma_1}, \dots, v_{\sigma_{m-n+1}}\}$ on $\text{Ker}(B)$. Define the winding map $\mathbf{w} : \mathbb{T}_0^n \rightarrow \text{Ker}'(B)$ by:

$$(2.2) \quad \mathbf{w}(\theta) = \frac{1}{2\pi} \sum_{i=1}^{m-n+1} (v_{\sigma_i}^\top d_G(\theta)) v'_{\sigma_i}.$$

The winding map \mathbf{w}_Σ in Definition (ii) is the representation of the map \mathbf{w} in equation (2.2) in the basis $\{v'_{\sigma_1}, \dots, v'_{\sigma_{m-n+1}}\}$ for $\text{Ker}'(B)$.

- (iv) Theorem 2.2(i) can be interpreted as the generalization of the classic Kirchhoff voltage law (KVL). For the graphs with nodal variables in \mathbb{R}^n , the KVL states that sum of the nodal differences along a cycle is 0. For graphs with nodal variables in n -torus, the sum of the nodal differences along a cycle is equal to $2\pi w$, where $w \in \mathbb{Z}$ is the winding number of the cycle.
- (v) We refer to [21, 14, 24] for key results and a survey on algorithms and computational complexity of computing integral and minimum cycle bases.

In order to illustrate the Kirchhoff angle law and various properties in Theorem 2.2, we get back to the polygonal graphs in Figure 1.1. We consider the square graph with a diagonal edge and define its cycles $\sigma_1 = (1, 2, 4, 1)$, $\sigma_2 = (2, 3, 4, 2)$, and $\sigma_3 = (1, 2, 3, 4, 1)$, as in Figure 1.1. Note that only two cycles are independent in the sense that the signed cycle vectors satisfy $v_{\sigma_1} + v_{\sigma_2} = v_{\sigma_3}$ and so the set $\Sigma = \{v_{\sigma_1}, v_{\sigma_2}\}$ is a basis for cycle space of G . The winding map of the graph G with respect to basis Σ is given by $\mathbf{w}_\Sigma(\theta) = [w_{\sigma_1} \ w_{\sigma_2}]^\top$. Theorem 2.2(i) implies that $|w_{\sigma_i}(\theta)| \leq \lceil \frac{3}{2} \rceil - 1 = 1$, for every $\theta \in \mathbb{T}_0^4$ and every $i \in \{1, 2\}$. Therefore, $\text{Img}(\mathbf{w}_\Sigma) \subseteq \{-1, 0, +1\}^2$. Moreover, the winding vectors $[1 \ 1]^\top$ and $[-1 \ -1]^\top$ are not possible for the square graph with a diagonal. This implies that $\text{Img}(\mathbf{w}_\Sigma) \subset \{-1, 0, +1\}^2$ and therefore, in general, the inclusion in Theorem 2.2(iii) can be strict.

We have now completed our study of the winding vector and so we are ready to introduce a new concept.

DEFINITION 2.4 (Winding cell). Consider the cyclic connected undirected graph G with cycle basis $\Sigma = \{\sigma_1, \dots, \sigma_{m-n+1}\}$ and associated winding map $\mathbf{w}_\Sigma : \mathbb{T}_0^n \rightarrow \mathbb{Z}^{m-n+1}$. For $\mathbf{u} \in \text{Img}(\mathbf{w}_\Sigma)$, the \mathbf{u} -winding cell is the set $\Omega_{\mathbf{u}}^G \subseteq \mathbb{T}_0^n$ defined by

$$\Omega_{\mathbf{u}}^G = \mathbf{w}_\Sigma^{-1}(\mathbf{u}).$$

Moreover, the reduced \mathbf{u} -winding cell is $\Omega_{\mathbf{u}}^G/\mathbb{S}^1$.

We are now ready to state the main result of this section. Since the $\text{Img}(\mathbf{w}_\Sigma)$ is a finite set, we now show how to partition the set \mathbb{T}_0^n into a finite number of regions.

THEOREM 2.5 (Winding partition of the n -torus). *Consider a connected cyclic undirected graph G with cycle basis $\Sigma = \{\sigma_1, \dots, \sigma_{m-n+1}\}$. Let \mathbf{w}_Σ be the corresponding winding map. Then the set $\{\text{closure}(\Omega_{\mathbf{u}}^G) \mid \mathbf{u} \in \text{Img}(\mathbf{w}_\Sigma)\}$ is a partition of \mathbb{T}^n , called the G -winding partition of \mathbb{T}^n , in the sense that*

(i) $\mathbb{T}^n = \bigcup_{\mathbf{u} \in \text{Img}(\mathbf{w}_\Sigma)} \text{closure}(\Omega_{\mathbf{u}}^G)$;

(ii) for every $\mathbf{u}, \mathbf{v} \in \text{Img}(\mathbf{w}_\Sigma)$ such that $\mathbf{u} \neq \mathbf{v}$, we have $\Omega_{\mathbf{u}}^G \cap \Omega_{\mathbf{v}}^G = \emptyset$;

Proof. Regarding part (i), it is clear that, for every $\mathbf{u} \in \text{Img}(\mathbf{w}_\Sigma)$, we have $\Omega_{\mathbf{u}}^G \subset \mathbb{T}_0^n$. This implies that $\bigcup_{\mathbf{u} \in \text{Img}(\mathbf{w}_\Sigma)} \Omega_{\mathbf{u}}^G \subseteq \mathbb{T}_0^n$. Moreover, for every $\theta \in \mathbb{T}_0^n$, we have $\theta \in \Omega_{\mathbf{w}_\Sigma(\theta)}^G$. Therefore, we have $\bigcup_{\mathbf{u} \in \text{Img}(\mathbf{w}_\Sigma)} \Omega_{\mathbf{u}}^G = \mathbb{T}_0^n$. Finally, by taking closure of both side of this equality and noting that $\text{closure}(\mathbb{T}_0^n) = \mathbb{T}^n$, we get

$$\bigcup_{\mathbf{u} \in \text{Img}(\mathbf{w}_\Sigma)} \text{closure}(\Omega_{\mathbf{u}}^G) = \mathbb{T}^n.$$

Regarding part (ii), suppose that for some $\mathbf{u} \neq \mathbf{v}$, we have $\theta \in \Omega_{\mathbf{u}}^G \cap \Omega_{\mathbf{v}}^G$. Then, $\mathbf{w}_\Sigma(\theta) = \mathbf{u} = \mathbf{v}$, which is a contradiction. Therefore, we have $\Omega_{\mathbf{u}}^G \cap \Omega_{\mathbf{v}}^G = \emptyset$. \square

For the triangle graph in Figure 1.1, one can visualize the winding cells. Note that the triangle graph with only cycle $\sigma = (1, 2, 3, 1)$ has $\text{Img}(\mathbf{w}_\Sigma) = \{-1, 0, +1\}$. Therefore, the winding cells of \mathbb{T}_0^3 are

$$\Omega_{-1}^G = \{\theta = (\theta_1, \theta_2, \theta_3)^\top \in \mathbb{T}_0^3 \mid v_\sigma^\top d_G(\theta) = -2\pi\},$$

$$\Omega_0^G = \{\theta = (\theta_1, \theta_2, \theta_3)^\top \in \mathbb{T}_0^3 \mid \text{there exists an arc of length } \pi \text{ containing } \theta_1, \theta_2, \theta_3\},$$

$$\Omega_1^G = \{\theta = (\theta_1, \theta_2, \theta_3)^\top \in \mathbb{T}_0^3 \mid v_\sigma^\top d_G(\theta) = 2\pi\}.$$

Figure 2.2 illustrates these winding cells.

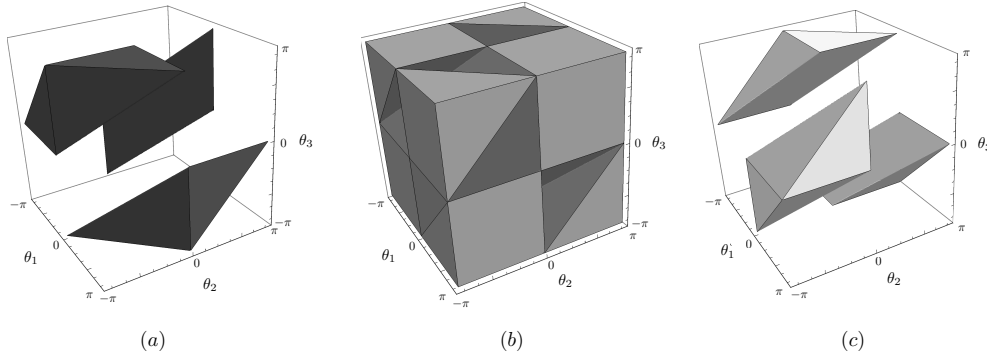


Fig. 2.2: The winding cells Ω_{-1}^G , Ω_0^G , and Ω_1^G , induced by the triangle graph on \mathbb{T}_0^3 are shown in Figures (a), (b), and (c), respectively. The three axes represent the three angles $\theta_1, \theta_2, \theta_3$, on the interval $[-\pi, \pi)$. These axes are periodic on the 3-torus, so all three winding cells are path-connected, despite their disconnected representations in \mathbb{R}^3 .

Next we present more properties of the winding cells.

THEOREM 2.6 (Polytopic characterization of winding cells). *Consider a connected cyclic undirected graph G with cycle basis $\Sigma = \{\sigma_1, \dots, \sigma_{m-n+1}\}$. Let \mathbf{w}_Σ and $C_\Sigma \in \mathbb{R}^{(m-n+1) \times m}$ be the corresponding winding map and cycle-edge matrix. For $\mathbf{u} \in \text{Img}(\mathbf{w}_\Sigma)$, define the open convex polytope*

$$P_{\mathbf{u}} = \{\mathbf{x} \in \mathbb{1}_n^\perp \mid \|B^\top \mathbf{x} + 2\pi C_\Sigma^\dagger \mathbf{u}\|_\infty < \pi\}.$$

Then the following statements hold:

(i) there exists a bijection $\iota : \Omega_{\mathbf{u}}^G/\mathbb{S}^1 \rightarrow P_{\mathbf{u}}$ satisfying, for all $\theta \in \Omega_{\mathbf{u}}^G$,

$$d_G(\theta) = B^\top \iota([\theta]) + 2\pi C_\Sigma^\dagger \mathbf{u};$$

(ii) the winding cell $\Omega_{\mathbf{u}}^G$ is a connected component of \mathbb{T}_0^n .

Proof. Regarding part (i), fix $\theta \in \Omega_{\mathbf{u}}^G \subset \mathbb{T}_0^n$. By Theorem 2.2(ii), for every cycle σ , we have $w_\sigma(\theta) = \frac{1}{2\pi} v_\sigma^\top d_G(\theta)$. Applying this formula to every cycle in the cycle basis Σ , we get $\mathbf{u} = \mathbf{w}_\Sigma(\theta) = \frac{1}{2\pi} C_\Sigma d_G(\theta)$. In turn, by Lemma A.1(ii), we have $\text{Ker}(C_\Sigma) = \text{Img}(B^\top)$. This implies that there exists a unique $\mathbf{x} \in \mathbb{1}_n^\perp$ such that $d_G(\theta) = B^\top \mathbf{x} + 2\pi C_\Sigma^\dagger \mathbf{u}$. Now we can define the map $\iota : \Omega_{\mathbf{u}}^G/\mathbb{S}^1 \rightarrow P_{\mathbf{u}}$ by

$$\iota([\theta]) = \mathbf{x},$$

where $\mathbf{x} \in \mathbb{1}_n^\perp$ is such that $d_G(\theta) = B^\top \mathbf{x} + 2\pi C_\Sigma^\dagger \mathbf{u}$. We show that ι is a one-to-one correspondence between $\Omega_{\mathbf{u}}^G/\mathbb{S}^1$ and $P_{\mathbf{u}}$. Consider the linear equations

$$(2.3) \quad C_\Sigma \mathbf{z} = \mathbf{u}.$$

By Lemma A.1(iii), the system of linear equations (2.3) has an integer solution \mathbf{z} . Since $C_\Sigma^\dagger \mathbf{u}$ is another solution for (2.3) and $\text{Ker}(C_\Sigma) = \text{Img}(B^\top)$, there exists $\alpha \in \mathbb{1}_n^\perp$ such that $\mathbf{z} - C_\Sigma^\dagger \mathbf{u} = B^\top \alpha$. Now, we define the open set $D = \{\mathbf{x} \in \mathbb{1}_n^\perp \mid \|B^\top \mathbf{x} + 2\pi C_\Sigma^\dagger \mathbf{u}\|_\infty < \pi\}$. We first show that the map ι is injective. Suppose that $[\theta_1], [\theta_2] \in \Omega_{\mathbf{u}}^G/\mathbb{S}^1$ are such that $\iota([\theta_1]) = \iota([\theta_2]) = \mathbf{x}$. This implies that $d_G(\theta_1) = d_G(\theta_2) = B^\top \mathbf{x} + 2\pi C_\Sigma^\dagger \mathbf{u}$ and as a result, we get $\theta_1 = \text{rot}_s(\theta_2)$, for some $s \in [0, 2\pi)$. This completes the proof of the fact that ι is injective. Now we show that ι is surjective. Let $\mathbf{x} \in D$. Then we define $\theta \in \mathbb{S}^1$ by

$$\theta = \text{mod}(\mathbf{x} - 2\pi\alpha, 2\pi).$$

Suppose that $e = (i, j) \in \mathcal{E}$. Then we have

$$(d_G(\theta))_e = d_{cc}(\theta_i, \theta_j) = (x_i - 2\pi\alpha_i) - (x_j - 2\pi\alpha_j) + 2\pi z_i,$$

where the second equality is because of the fact that

$$|(x_i - 2\pi\alpha_i) - (x_j - 2\pi\alpha_j) + 2\pi z_i| \leq \|B^\top \mathbf{x} - 2\pi\alpha + 2\pi\mathbf{z}\|_\infty = \|B^\top \mathbf{x} + 2\pi C_\Sigma^\dagger \mathbf{u}\|_\infty < \pi.$$

Therefore, we have

$$d_G(\theta) = B^\top (\mathbf{x} - 2\pi\alpha) + 2\pi\mathbf{z} = B^\top \mathbf{x} + 2\pi C_\Sigma^\dagger \mathbf{u}.$$

This implies that $\iota([\theta]) = \mathbf{x}$ and completes the surjectivity of the map ι . This completes the proof of part (i).

Regarding part (ii), note that the set $D \subset \mathbb{1}_n^\perp$ given by

$$D = \{\mathbf{x} \in \mathbb{1}_n^\perp \mid \|B^\top \mathbf{x} + 2\pi C_\Sigma^\dagger \mathbf{u}\|_\infty < \pi\}$$

is connected in $\mathbb{1}_n^\perp$. Suppose that $\theta, \eta \in \Omega_{\mathbf{u}}^G$. Then we set $\mathbf{x}_1 = \iota([\theta])$ and $\mathbf{x}_2 = \iota([\eta])$. We set $\gamma := \max\{\|B^\top \mathbf{x}_1 + 2\pi C_\Sigma^\dagger \mathbf{u}\|_\infty, \|B^\top \mathbf{x}_2 + 2\pi C_\Sigma^\dagger \mathbf{u}\|_\infty\}$ and define $D_\gamma = \{\mathbf{x} \in \mathbb{1}_n^\perp \mid \|B^\top \mathbf{x} + 2\pi C_\Sigma^\dagger \mathbf{u}\|_\infty < \gamma\}$. Then using the same argument as in the proof of part (i), the map ι induces a one-to-one correspondence between $\Omega_{\mathbf{u}}^G \cap \Delta^G(\gamma)$ and the set D_γ , modulo rotations. Since $\Omega_{\mathbf{u}}^G \cap \Delta^G(\gamma)$ is compact in \mathbb{T}^n and ι is continuous, this implies that ι is a homeomorphism. Therefore, the curve $\iota^{-1} \circ \xi : [0, 1] \rightarrow \Omega_{\mathbf{u}}^G$ is a continuous and we have $\iota^{-1} \circ \xi(0) = [\theta]$ and $\iota^{-1} \circ \xi(1) = [\eta]$. Thus, $\Omega_{\mathbf{u}}^G$ is a connected component of \mathbb{T}^n . \square

In Figure 2.3, we plot the reduced winding cells $\Omega_{-1}^G/\mathbb{S}^1$, Ω_0^G/\mathbb{S}^1 , and Ω_1^G/\mathbb{S}^1 induced by the triangle graph and square graph on \mathbb{T}_0^3 and \mathbb{T}_0^4 , respectively. Figure 2.3 plots the winding cells as functions of counterclockwise distances $d_{cc}(\theta_i, \theta_{i+1})$ rather than phases θ_i , effectively modding out uniform rotations.

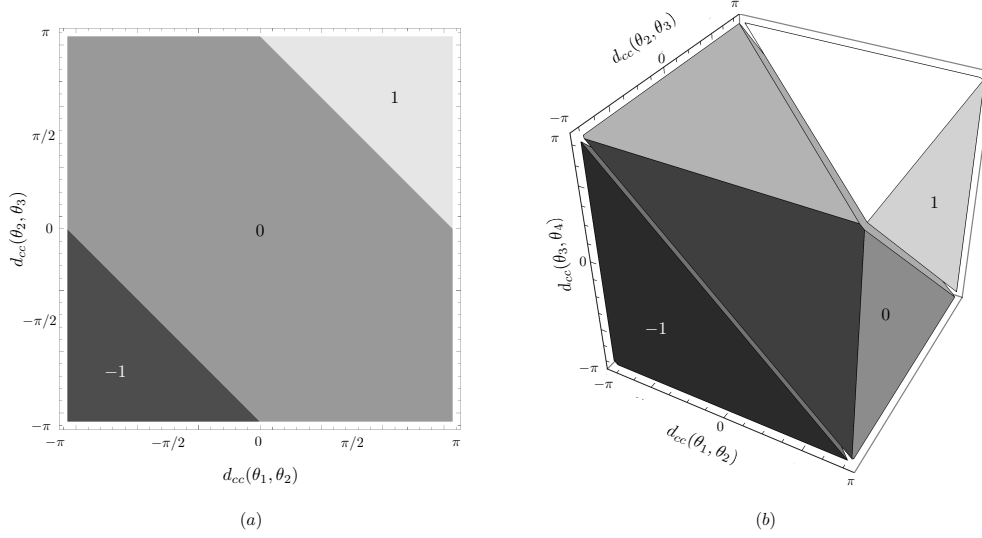


Fig. 2.3: The reduced winding cells induced by the triangle graph (a) and square graph (b) on \mathbb{T}_0^3 and \mathbb{T}_0^4 , respectively. In both plots, each axis corresponds to one edge in the graph, indicating the counter-clockwise distance between the incident nodes, on the interval $[-\pi, \pi]$.

While the winding map \mathbf{w}_Σ in Definition 2.1 (iii) depends on the cycle basis Σ , the winding partition of \mathbb{T}^m in Theorem 2.5 is independent of the basis Σ , in the sense that, given any other cycle basis Σ' , each winding cell $\Omega_{\mathbf{u}}^G$, for $\mathbf{u} \in \text{Img}(\mathbf{w}_\Sigma)$, is equal to a cell $\Omega_{\mathbf{u}'}^G$ defined by an appropriate $\mathbf{u}' \in \text{Img}(\mathbf{w}_{\Sigma'})$.

We can obtain an upper bound on the cardinality of the winding partition as follows. First, Theorem 2.2(iii) gives a superset of $\text{Img}(\mathbf{w}_\Sigma)$ and, therefore, provides the upper bound

$$|\text{Img}(\mathbf{w}_\Sigma)| \leq \prod_{i=1}^{|\Sigma|} (2\lceil n_{\sigma_i}/2 \rceil - 1) \leq \prod_{i=1}^{|\Sigma|} (n_{\sigma_i} + 1) \leq \left(\frac{\sum_{i=1}^{|\Sigma|} (n_{\sigma_i} + 1)}{|\Sigma|} \right)^{|\Sigma|},$$

where $|\Sigma| = m - n + 1$, and we used $2\lceil n_{\sigma}/2 \rceil - 1 \leq n_{\sigma} + 1$ and the inequality of arithmetic and geometric means. Now, the classic result [21, Theorem 6] states that the length of a minimum cycle bases of an unweighted graph is at most $3(n-1)(n-2)/2$, so that

$$|\text{Img}(\mathbf{w}_\Sigma)| \leq \left(\frac{3(n-1)(n-2)}{m-n+1} + 1 \right)^{m-n+1}.$$

Alternatively, the length of minimum cycle basis of an unweighted graph is known [14] to be in $\mathcal{O}(m \log(n) \log(\log(n)))$ so that there exists a constant C such that

$$|\text{Img}(\mathbf{w}_\Sigma)| \leq (C \log n \log \log n)^{m-n+1}.$$

If the graph admits a basis of cycles with length at most n_σ , then

$$|\text{Img}(\mathbf{w}_\Sigma)| \leq (2\lceil n_\sigma/2 \rceil - 1)^{m-n+1}.$$

For example, the complete graph K_n has a cycle basis with $n_\sigma = 3$ and so, given $m - n + 1 = (n-1)(n-2)/2$, we know $|\text{Img}(\mathbf{w}_\Sigma)| \leq 3^{(n-1)(n-2)/2}$. The two-dimensional grid graph $G_{h,k}$ with $n = hk$ nodes and $m = 2hk - h - k$ edges, has a cycle basis with $n_\sigma = 4$ so that $|\text{Img}(\mathbf{w}_\Sigma)| \leq 3^{hk-h-k+1}$.

3. At-most uniqueness of active power flows in each winding cell. In

this section we apply the winding partition and its properties to study the following problem.

DEFINITION 3.1 (Active power flow problem). *Let G be a weighted undirected graph with n nodes, m edges, incidence matrix B , and edge weight matrix \mathcal{A} . Let $p_{\text{sd}} \in \mathbb{1}_n^\perp$ be a balanced supply/demand vector. The active power flow problem is to find angles $\theta \in \mathbb{T}^n$ and flows $f \in \mathbb{R}^m$ such that*

$$(3.1a) \quad p_{\text{sd}} = Bf,$$

$$(3.1b) \quad f = \mathcal{A} \sin(B^\top \theta).$$

Equation (3.1a) is a *flow conservation law* and equation (3.1b) is known as the *power angle equation* (the flow of active power on a AC line is proportional to the power angle, i.e., the phase difference between the two nodes). We refer to the combined equations (3.1) as to the *active power flow equations*; clearly they are equivalent to

$$(3.2) \quad p_{\text{sd}} = B\mathcal{A} \sin(B^\top \theta).$$

A phase angle $\theta \in \mathbb{T}^n$ satisfying equations (3.2) is called a *stable* solution of the active power flow equations if $|\theta_i - \theta_j| < \frac{\pi}{2}$, for every edge (i, j) of G .

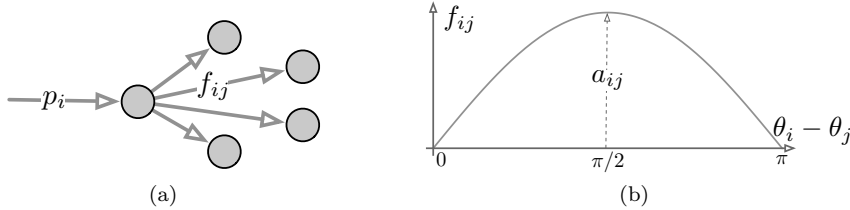


Fig. 3.1: Interpretation of the active power flow equations (3.2). Figure (a) illustrates that the active power satisfies a conservation law at each node: $p_i = \sum_{j=1}^n f_{ij}$. Figure (b) shows the proportional relationship between the active power transferred along an edge and the sine of its angle difference.

- REMARKS 3.2.** (i) *We assume G to be connected (without loss of generality) and cyclic (because the active problem flow problem over a tree is trivial [12]).*
(ii) *The active power flow problem is identical to the problem of computing equilibrium points for the celebrated Kuramoto model of coupled oscillators*

$$(3.3) \quad \dot{\theta}_i = \sum_{j=1}^n a_{ij} \sin(\theta_i - \theta_j),$$

and for the coupled swing equations in power systems

$$(3.4) \quad M_i \ddot{\theta}_i + d_i \dot{\theta}_i = \sum_{j=1}^n a_{ij} \sin(\theta_i - \theta_j).$$

Moreover, a stable solution of the active power flow equation is a locally asymptotically stable equilibrium point of the Kuramoto model and locally asymptotically stable equilibrium configuration of the coupled swing equations, modulo rotations. Note that the converse is not true; there might exist stable equilibrium points for the swing equations or Kuramoto model for which $|\theta_i - \theta_j| \geq \frac{\pi}{2}$, for some edge (i, j) of G . However, these equilibrium points are of limited practical interest for power networks.

- (iii) The active power flow equations model power flow in AC circuits based on the following simplifications: the lines are purely inductive (without losses) and network voltages are constant. Under these assumptions the edge $\{i, j\}$ has weight $a_{ij} = V_i V_j Y_{ij}$, where $-Y_{ij}$ is the line susceptance and V_i, V_j are the voltage magnitudes at nodes i and j .
- (iv) In practice, the power transmitted on a power line is limited by thermal constraints. Such thermal constraints may be expressed as the upper bound

$$(3.5) \quad \|\sin(B^\top \theta)\|_\infty \leq \sin(\gamma),$$

for some maximum angle $\gamma \in [0, \frac{\pi}{2})$. As documented in [47, Section 2.2.3], 100% utilization is rarely achievable, the utilization ratio of 90% is considered a physical threshold, and utilization ratios below 75% are often encountered.

The thermal constraints (3.5) motivates the following definition.

DEFINITION 3.3 (Phase-cohesive set and phase-cohesive winding cells). For an angle $\gamma \in [0, \pi)$, the γ -phase-cohesive set $\Delta^G(\gamma) \subseteq \mathbb{T}_0^n$ is

$$\Delta^G(\gamma) = \{\theta \in \mathbb{T}^n \mid |\theta_i - \theta_j| \leq \gamma \text{ for each } (i, j) \in \mathcal{E}\}$$

and, for winding vector $\mathbf{u} \in \text{Img}(\mathbf{w}_\Sigma)$, the phase-cohesive \mathbf{u} -winding cell is

$$\Omega_{\mathbf{u}}^G(\gamma) = \Omega_{\mathbf{u}}^G \cap \Delta^G(\gamma) = \{\theta \in \mathbb{T}^n \mid \mathbf{w}_\Sigma(\theta) = \mathbf{u} \text{ and } |\theta_i - \theta_j| \leq \gamma \text{ for each } (i, j) \in \mathcal{E}\}.$$

Moreover, the reduced phase-cohesive \mathbf{u} -winding cell is $\Omega_{\mathbf{u}}^G(\gamma)/\mathbb{S}^1$.

In Figure (3.2), for $\gamma = 1.5$, we plot the reduced γ -phase-cohesive winding cells $\Omega_{-1}^G(\gamma)/\mathbb{S}^1$, $\Omega_0^G(\gamma)/\mathbb{S}^1$, and $\Omega_1^G(\gamma)/\mathbb{S}^1$, induced by the triangle graph and square graph on \mathbb{T}_0^3 and \mathbb{T}_0^4 , respectively. Figure (3.2) plots these cells as functions of counterclockwise distances $d_{cc}(\theta_i, \theta_{i+1})$ rather than phases θ_i , effectively modding out uniform rotations.

By definition, if θ is in the γ -phase-cohesive set, then it satisfies the thermal constraints (3.5). The following results are immediate consequences of Theorem 2.5.

LEMMA 3.4 (Phase-cohesive winding partition). Pick an angle $\gamma \in [0, \pi)$,

- (i) for $\mathbf{u} \in \text{Img}(\mathbf{w}_\Sigma)$, the phase-cohesive winding cell $\Omega_{\mathbf{u}}^G(\gamma)$ is a connected component of $\Delta^G(\gamma)$ and there exists a one-to-one correspondence between the reduced phase-cohesive \mathbf{u} -winding cell and

$$\{\mathbf{x} \in \mathbb{1}_n^\perp \mid \|B^\top \mathbf{x} + 2\pi C^\dagger_\Sigma \mathbf{u}\|_\infty < \gamma\},$$

- (ii) the set $\{\Omega_{\mathbf{u}}^G(\gamma) \mid \mathbf{u} \in \text{Img}(\mathbf{w}_\Sigma)\}$ is a partition of $\Delta^G(\gamma)$, called the phase-cohesive winding partition, in the sense that

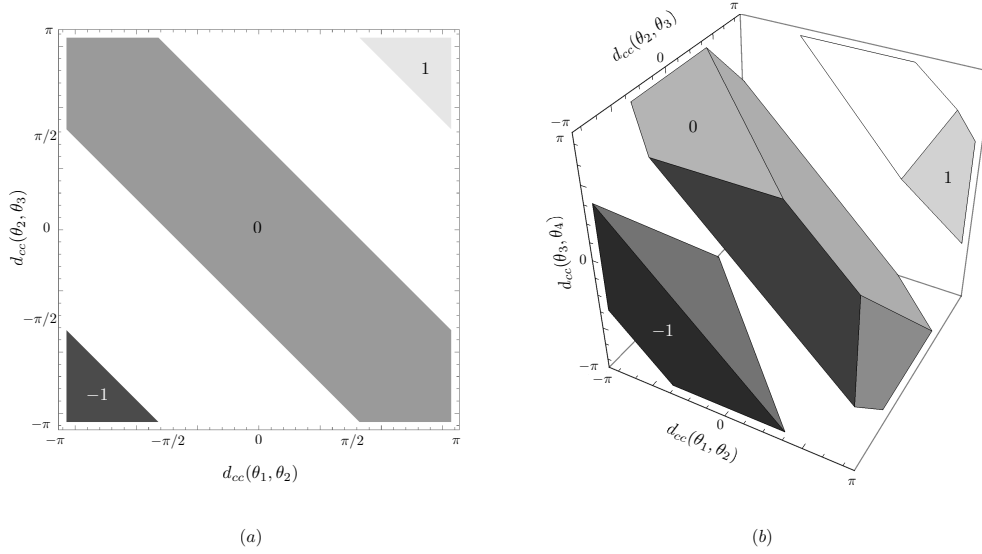


Fig. 3.2: The reduced γ -phase-cohesive winding cells ($\gamma = 1.5$) induced by the triangle graph (a) and square graph (b) on \mathbb{T}_0^3 and \mathbb{T}_0^4 , respectively. In both plots, each axis corresponds to one edge in the graph, indicating the counter-clockwise distance between the incident nodes, on the interval $[-\pi, \pi)$.

$$(a) \quad \Delta^G(\gamma) = \bigcup_{\mathbf{u} \in \text{Img}(\mathbf{w}_\Sigma)} \Omega_{\mathbf{u}}^G(\gamma);$$

$$(b) \quad \text{for every } \mathbf{u}, \mathbf{v} \in \text{Img}(\mathbf{w}_\Sigma) \text{ such that } \mathbf{u} \neq \mathbf{v}, \text{ we have } \Omega_{\mathbf{u}}^G(\gamma) \cap \Omega_{\mathbf{v}}^G(\gamma) = \emptyset.$$

The following simple example illustrates how the active power flow equations (3.2) can have multiple solutions inside the phase-cohesive set.

Consider the active power flow equations (3.2) over the unit-weighted pentagon graph in Figure 1.1. For $p_{\text{sd}} = \mathbf{0}_5$, one can check that there exists two solutions $\phi, \psi \in \Delta^G(\pi/2) \subset \mathbb{T}^5$ to equations (3.2) given by $\phi = \mathbf{0}_5$ and $\psi = (0, \frac{2\pi}{5}, \frac{4\pi}{5}, \frac{6\pi}{5}, \frac{8\pi}{5})^\top$, and that they have different winding number along the cycle $\sigma = (1, 2, 3, 4, 5)$:

$$w_\sigma(\phi) = \frac{1}{2\pi} \sum_{i=1}^5 d_{\text{cc}}(\phi_i, \phi_{i+1}) = 0, \quad \text{and} \quad w_\sigma(\psi) = \frac{1}{2\pi} \sum_{i=1}^5 \frac{2\pi}{5} = 1.$$

We are now ready to state the main result of this section: the active power flow equations have at most one solution inside each phase-cohesive winding cell.

THEOREM 3.5 (At most uniqueness of stable power flow solutions in each phase-cohesive winding cell). *Consider the active power flow equation (3.2) defined over a cyclic connected undirected graph G with incidence matrix B , edge weight matrix A , cycle basis Σ , and cycle projection matrix \mathcal{P}_{cyc} . For any angle $\gamma \in [0, \frac{\pi}{2})$, winding vector $\mathbf{u} \in \text{Img}(\mathbf{w}_\Sigma)$, and balanced power supply/demand vector $p_{\text{sd}} \in \mathbb{1}_n^\perp$, there exists at most one stable solution of equation (3.2), modulo rotations, inside the phase-cohesive winding cell $\Omega_{\mathbf{u}}^G(\gamma)$*

Proof. Assume there exist two angle arrays $\phi, \psi \in \Omega_{\mathbf{u}}^G(\gamma)$ satisfying the active power flow equations (3.2). Then $\|d_G(\phi)\|_\infty, \|d_G(\psi)\|_\infty \leq \gamma$. Note that \sin is a strictly

increasing function on the interval $[-\frac{\pi}{2}, \frac{\pi}{2}]$. Thus

$$\begin{aligned} (d_G(\phi) - d_G(\psi))^\top \mathcal{A}(\sin(d_G(\phi)) - \sin(d_G(\psi))) \\ = \sum_{e \in \mathcal{E}} a_e (d_G^e(\phi) - d_G^e(\psi)) (\sin(d_G^e(\phi)) - \sin(d_G^e(\psi))) \geq 0, \end{aligned}$$

and the equality holds if and only if $d_G(\phi) = d_G(\psi)$. Now, Theorem 2.5(i) implies that there exist $\mathbf{x}, \mathbf{x}' \in \mathbf{1}_n^\perp$ such that

$$d_G(\phi) = B^\top \mathbf{x} + 2\pi C_\Sigma^\dagger \mathbf{u}, \quad d_G(\psi) = B^\top \mathbf{x}' + 2\pi C_\Sigma^\dagger \mathbf{u}.$$

As a result, we obtain

$$\begin{aligned} (d_G(\phi) - d_G(\psi))^\top \mathcal{A}(\sin(d_G(\phi)) - \sin(d_G(\psi))) \\ = (B^\top (\mathbf{x} - \mathbf{x}'))^\top \mathcal{A}(\sin(d_G(\phi)) - \sin(d_G(\psi))) \\ = (\mathbf{x} - \mathbf{x}')^\top B \mathcal{A}(\sin(d_G(\phi)) - \sin(d_G(\psi))). \end{aligned}$$

Since ϕ, ψ are solutions to the power flow equations (3.2), we compute

$$B \mathcal{A}(\sin(d_G(\phi)) - \sin(d_G(\psi))) = p_{\text{sd}} - p_{\text{sd}} = \mathbf{0}_n.$$

This implies that $(d_G(\phi) - d_G(\psi))^\top \mathcal{A}(\sin(d_G(\phi)) - \sin(d_G(\psi))) = \mathbf{0}_n$. Therefore, we have $d_G(\phi) = d_G(\psi)$ and, in turn, $\phi = \text{rot}_s(\psi)$ for some $s \in [0, 2\pi)$. This completes the proof of the theorem. \square

The following result applies to the complete graphs, complete bipartite graphs, and two-dimensional grids, see Figure 3.3.

COROLLARY 3.6 (Graphs with a basis of short cycles). *Under the assumptions of Theorem 3.5, for any graph G with a cycle basis of maximum length at most 4, the following statements hold:*

- (i) *the phase-cohesive winding partition in Lemma 3.4(ii) is composed of the single winding cell $\Omega_{\mathbf{0}}^G(\gamma)$ associated to the zero winding vector, and*
- (ii) *the active power flow equations (3.2) have at most one solution, modulo rotations, in the phase-cohesive set $\Delta^G(\gamma)$.*

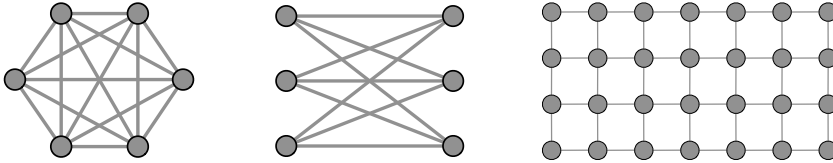


Fig. 3.3: Corollary 3.6 implies that complete graphs, complete bipartite graphs, and two-dimensional grid graphs have at most one stable active power flow solution, independently of supply/demand vector and edge weights.

We conclude this section by studying the properties of the power flow solutions.

THEOREM 3.7 (Properties of power flow at solution). *Consider the active power flow equations (3.1) defined on an undirected weighted graph G with the incidence matrix B , edge weight matrix \mathcal{A} , and the cycle basis Σ . Assume a solution (f, θ) exists at power supply/demand $p_{\text{sd}} \in \mathbf{1}_n^\perp$. Then*

(i) the power flow f can be decomposed uniquely as

$$f = f_{\text{cut}} + f_{\text{cyc}},$$

where $f_{\text{cut}} = B^\top(BB^\top)^\dagger p_{\text{sd}} \in \text{Img}(B^\top)$ is called the cutset flow and $f_{\text{cyc}} \in \text{Ker}(B)$ is called the cycle flow.

Moreover, for any angle $\gamma \in [0, \frac{\pi}{2})$, if $\phi, \psi \in \mathbb{T}^n$ are two solutions of the active power flow equations (3.2) in $\Delta^G(\gamma)$ with power flow vectors $f_\phi = \mathcal{A}\sin(B^\top\phi)$ and $f_\psi = \mathcal{A}\sin(B^\top\psi)$, then

- (ii) $f_\phi - f_\psi \in \text{Ker}(B)$, that is, power flow solutions differ by a cycle flow;
- (iii) $f_\phi = f_\psi$ if and only if $\mathbf{w}_\Sigma(\phi) = \mathbf{w}_\Sigma(\psi)$ if and only if $\phi = \text{rot}_s(\psi)$, for some $s \in [0, 2\pi)$;
- (iv) if G has exactly one cycle σ , then

$$w_\sigma(\phi) > w_\sigma(\psi) \iff v_\sigma^\top f_\phi > v_\sigma^\top f_\psi,$$

that is, the equilibrium loop flows are monotone with respect to winding numbers.

Proof. Regarding part (i), note that $\text{Img}(B^\top) \oplus \text{Ker}(B) = \mathbb{R}^m$. Therefore, there exists a unique decomposition $f = f_{\text{cut}} + f_{\text{cyc}}$, where $f_{\text{cut}} \in \text{Img}(B^\top)$ and $f_{\text{cyc}} \in \text{Ker}(B)$. Additionally, the power flow f satisfies the active power flow equations (3.1), that is $Bf = p_{\text{sd}}$. Note that $f_{\text{cyc}} \in \text{Ker}(B)$ and this implies that $Bf_{\text{cut}} = p_{\text{sd}}$. Moreover, $f_{\text{cut}} \in \text{Img}(B^\top)$ and therefore there exists $x \in \mathbb{1}_n^\perp$ such that $f_{\text{cut}} = B^\top x$. This implies that $BB^\top x = p_{\text{sd}}$. Finally, one can compute $f_{\text{cut}} = B^\top x = B^\top(BB^\top)^\dagger p_{\text{sd}}$. This completes the proof of part (i).

Regarding part (ii), note that, we have $p_{\text{sd}} = Bf_\phi = Bf_\psi$. This implies that $B(f_\phi - f_\psi) = 0$ and in turn $f_\phi - f_\psi \in \text{Ker}(B)$.

Regarding part (iii), consider $f_\phi = \mathcal{A}\sin(B^\top\phi)$ and $f_\psi = \mathcal{A}\sin(B^\top\psi)$. Given $\phi = \psi$, it is trivial to see that $f_\phi = f_\psi$. Now suppose that, for ϕ, ψ , we have $f_\phi = f_\psi$. Since $\phi, \psi \in \Delta^G(\gamma)$, we have $d_G(\phi) = \arcsin(\sin(B^\top\phi))$ and $d_G(\psi) = \arcsin(\sin(B^\top\psi))$. Therefore, for every cycle σ ,

$$\begin{aligned} w_\sigma(\phi) &= \frac{1}{2\pi} v_\sigma^\top \arcsin(\sin(B^\top\phi)) = \frac{1}{2\pi} v_\sigma^\top \arcsin(\mathcal{A}^{-1}f_\phi), \\ w_\sigma(\psi) &= \frac{1}{2\pi} v_\sigma^\top \arcsin(\sin(B^\top\psi)) = \frac{1}{2\pi} v_\sigma^\top \arcsin(\mathcal{A}^{-1}f_\psi). \end{aligned}$$

This implies that ϕ must have the same winding vector as ψ .

Regarding part (iv), Since $\phi, \psi \in \Delta^G(\gamma)$, we have $\|d_G(\phi)\|_\infty \leq \gamma$ and $\|d_G(\psi)\|_\infty \leq \gamma$. Note that \sin is a strictly increasing function on the interval $[-\frac{\pi}{2}, \frac{\pi}{2}]$. As a result,

$$\begin{aligned} (3.6) \quad (d_G(\phi) - d_G(\psi))^\top \mathcal{A}(\sin(d_G(\phi)) - \sin(d_G(\psi))) \\ = \sum_{e \in \mathcal{E}} a_e (d_G^e(\phi) - d_G^e(\psi)) (\sin(d_G^e(\phi)) - \sin(d_G^e(\psi))) \geq 0. \end{aligned}$$

Moreover, by Theorem 2.5(i), there exists $\mathbf{x}, \mathbf{x}' \in \mathbb{1}_n^\perp$ such that

$$(3.7) \quad d_G(\phi) = B^\top \mathbf{x} + 2\pi C_\Sigma^\dagger w_\sigma(\phi), \quad d_G(\psi) = B^\top \mathbf{x}' + 2\pi C_\Sigma^\dagger w_\sigma(\psi).$$

Replacing (3.7) into (3.6), we get

$$\begin{aligned}
& (d_G(\phi) - d_G(\psi))^\top \mathcal{A}(\sin(d_G(\phi)) - \sin(d_G(\psi))) \\
&= (B^\top(\mathbf{x} - \mathbf{x}') + 2\pi C_\Sigma^\dagger(w_\sigma(\phi) - w_\sigma(\psi)))^\top \mathcal{A}(\sin(d_G(\phi)) - \sin(d_G(\psi))) \\
(3.8) \quad &= (B^\top(\mathbf{x} - \mathbf{x}'))^\top \mathcal{A}(\sin(d_G(\phi)) - \sin(d_G(\psi))) \\
(3.9) \quad &+ (2\pi C_\Sigma^\dagger(w_\sigma(\phi) - w_\sigma(\psi)))^\top \mathcal{A}(\sin(d_G(\phi)) - \sin(d_G(\psi))).
\end{aligned}$$

Note that the term (3.8) is

$$(B^\top(\mathbf{x} - \mathbf{x}'))^\top \mathcal{A}(\sin(d_G(\phi)) - \sin(d_G(\psi))) = (\mathbf{x} - \mathbf{x}')^\top B \mathcal{A}(\sin(d_G(\phi)) - \sin(d_G(\psi))).$$

Since ϕ, ψ are solutions for the active power flow equations (3.2), we get

$$B \mathcal{A}(\sin(d_G(\phi)) - \sin(d_G(\psi))) = p_{\text{sd}} - p_{\text{sd}} = \mathbf{0}_n.$$

Therefore, the term (3.8) is equal to zero. Moreover, since σ is the only cycle for G , we have $C_\Sigma^\dagger = \frac{1}{n} v_\sigma^\top$. Therefore, the term (3.9) can be written as

$$\begin{aligned}
& (2\pi C_\Sigma^\dagger(w_\sigma(\phi) - w_\sigma(\psi)))^\top \mathcal{A}(\sin(B^\top \mathbf{x}) - \sin(B^\top \mathbf{x}')) \\
&= \frac{1}{n} (w_\sigma(\phi) - w_\sigma(\psi)) v_\sigma^\top \mathcal{A}(\sin(B^\top \mathbf{x}) - \sin(B^\top \mathbf{x}')) \\
&= \frac{1}{n} (w_\sigma(\phi) - w_\sigma(\psi)) (v_\sigma^\top f_\phi - v_\sigma^\top f_\psi).
\end{aligned}$$

Therefore, the inequality (3.6) can be written as $\frac{1}{n} (w_\sigma(\phi) - w_\sigma(\psi)) (v_\sigma^\top f_\phi - v_\sigma^\top f_\psi) \geq 0$. This completes the proof of part (iv). \square

4. A complete solver for the active power flow problem. In this section, we propose an iteration to verify the existence and compute the solution of the active power flow equations inside a winding cell. Using this iteration, we present a complete solver for the active power flow equations (3.2) inside the region $\Omega_{\mathbf{u}}^G(\gamma)$, for $\gamma \in [0, \frac{\pi}{2}]$.

One of the well-studied methods to find the solutions of system of nonlinear equations is the Newton–Raphson method. Unfortunately, for the active power flow equations (3.2), the Newton–Raphson iteration comes with no global convergence guarantee. Consider for example the active power flow equations (3.2) over the unit-weighted pentagon graph in Figure 1.1. For $p_{\text{sd}} = \mathbf{0}_5$, the active power flow equations with underlying graph G have a solutions $\phi^* = \mathbf{0}_5$ with winding number 0 and a solution $\psi^* = (0, \frac{2\pi}{5}, \frac{4\pi}{5}, \frac{6\pi}{5}, \frac{8\pi}{5})^\top$ with winding number +1. Consider the sequence $\{x^{(n)}\}_{n \in \mathbb{Z}_{\geq 0}}$ defined by the Newton–Raphson iterations:

$$x^{(n+1)} = x^{(n)} - (B \mathcal{A} \text{diag}(\cos(B^\top x^{(n)})) B^\top)^\dagger B \mathcal{A} \sin(B^\top x^{(n)}),$$

with initial point $x^{(0)} = (0, \frac{\pi}{3}, \frac{\pi}{2}, \frac{2\pi}{3}, 0)^\top$. While $\mathbf{w}_\Sigma(x^{(0)}) = 0$, the Newton–Raphson iterations starting from $x^{(0)}$ converges to ϕ^* with winding number +1. This example illustrates how the winding vector is not preserved in Newton–Raphson iterations and thus the Newton–Raphson method is not consistent with the partition of the n -torus introduced in Theorem 2.5.

We start by proposing a novel equivalent transcription of the active power flow equations based on an edge utilization concept. For any winding vector $\mathbf{u} \in \text{Img}(\mathbf{w}_\Sigma)$

and balanced supply/demand vector p_{sd} , we define the \mathbf{u} -winding edge balance equations in the variable $\eta \in \mathbb{R}^m$ by

$$(4.1) \quad \begin{cases} B^\top L^\dagger p_{\text{sd}} = \mathcal{P}_{\text{cut}} \eta, & \|\eta\|_\infty \leq 1, \\ \mathcal{P}_{\text{cyc}}(\arcsin(\eta) - 2\pi C_\Sigma^\dagger \mathbf{u}) = \mathbf{0}_m. \end{cases}$$

Note that the flow vector in the active power flow equations (3.2) is $f = \mathcal{A} \sin(B^\top \theta)$ and, as we show in the next theorem, the variable $\eta \in \mathbb{R}^m$ in the edge balance equations (4.1) can be written as $\eta = \mathcal{A}^{-1} f$. Thus, η can be interpreted as a normalized flow vector.

The next theorem establishes the equivalence between the \mathbf{u} -winding edge balance equations (4.1) and the active power flow equations (3.2).

THEOREM 4.1 (Equivalence of node balance and edge balance equations). *Let G be a weighted undirected connected graph with the incidence matrix B , the cycle projection matrix \mathcal{P}_{cyc} , the cycle basis Σ , and the associated cycle-edge matrix C_Σ . Let $\gamma \in [0, \frac{\pi}{2}]$ and $\mathbf{u} \in \text{Im}(w_\Sigma)$. Then the following statements are equivalent:*

- (i) *the active power flow equations (3.2) have a unique solutions θ^* , modulo rotations, in $\Omega_{\mathbf{u}}^G(\gamma)$;*
- (ii) *the \mathbf{u} -winding edge balance equations (4.1) have a unique solution $\eta^* \in \mathbb{R}^m$ with $\|\eta^*\|_\infty \leq \sin(\gamma)$.*

Additionally, if any of the equivalent conditions (i) or (ii) hold, then $\eta^ = \sin(B^\top \theta^*)$.*

Proof. We start by noting that, for $\theta^* \in \mathbb{T}^n$, we have $\sin(B^\top \theta^*) = \sin(d_G(\theta^*))$.

Regarding (i) \implies (ii), note that, if $\theta^* \in \Omega_{\mathbf{u}}^G(\gamma)$ is a solution of the power flow equations (3.2), then we have $p_{\text{sd}} = B\mathcal{A} \sin(d_G(\theta^*))$. Now, we define $\eta^* = \sin(d_G(\theta^*))$. Since $\theta^* \in \Omega_{\mathbf{u}}^G(\gamma)$, we know that $|d_G(\theta^*)| \leq \gamma$. This implies that $\eta^* \in D_\infty(\mathbf{0}_m, \sin(\gamma))$. Now we show that η^* satisfies the \mathbf{u} -winding edge balance equations (4.1). Note that, by multiplying both side of the equality $p_{\text{sd}} = B\mathcal{A} \sin(d_G(\theta^*))$ by $B^\top L^\dagger$, we get

$$B^\top L^\dagger p_{\text{sd}} = B^\top L^\dagger B\mathcal{A} \sin(d_G(\theta^*)) = \mathcal{P}_{\text{cut}} \sin(d_G(\theta^*)) = \mathcal{P}_{\text{cut}} \eta^*.$$

Moreover, by taking arcsin from both side of the equality $\eta^* = \sin(d_G(\theta^*))$, we have $\arcsin(\eta^*) = d_G(\theta^*)$. Now, by Theorem 2.5(i), there exists $\mathbf{x} \in \mathbb{1}_n^\perp$ such that

$$\arcsin(\eta^*) = d_G(\theta^*) = B^\top \mathbf{x} + 2\pi C_\Sigma^\dagger \mathbf{u}.$$

This implies that $\arcsin(\eta^*) - 2\pi C_\Sigma^\dagger \mathbf{u} \in \text{Im}(B^\top)$ and therefore

$$\mathcal{P}_{\text{cyc}}(\arcsin(\eta^*) - 2\pi C_\Sigma^\dagger \mathbf{u}) = \mathbf{0}_m.$$

Regarding (ii) \implies (i), note that from (4.1), we get that $\arcsin(\eta^*) - 2\pi C_\Sigma^\dagger \mathbf{u} \in \text{Im}(B^\top)$. Therefore, there exists $\mathbf{x} \in \mathbb{1}_n^\perp$ such that $\arcsin(\eta^*) = B^\top \mathbf{x} + 2\pi C_\Sigma^\dagger \mathbf{u}$. Using Theorem 2.5(i), there exists $\theta^* \in \Omega_{\mathbf{u}}^G(\gamma)$ such that

$$d_G(\theta^*) = B^\top \mathbf{x} + 2\pi C_\Sigma^\dagger \mathbf{u} = \arcsin(\eta^*).$$

This implies that $\sin(d_G(\theta^*)) = \sin(\arcsin(\eta^*)) = \eta^*$. Therefore, by replacing back into equations (4.1), we get $B^\top L^\dagger p_{\text{sd}} = \mathcal{P}_{\text{cut}} \sin(d_G(\theta^*))$. Bu multiplying both side of this equation by $B\mathcal{A}$, and using the fact that $p_{\text{sd}} \in \mathbb{1}_n^\perp$, we get $p_{\text{sd}} = B\mathcal{A} \sin(d_G(\theta^*))$. This equality completes the proof of the theorem. \square

Next, we introduce two useful notions. For every $\gamma \in [0, \frac{\pi}{2})$, define the scalar function $\arcsin_\gamma : \mathbb{R} \rightarrow \mathbb{R}$ by

$$\arcsin_\gamma(x) = \begin{cases} \frac{1}{\cos(\gamma)}x - \gamma + \tan(\gamma), & \text{if } x < -\sin(\gamma), \\ \arcsin(x), & \text{if } |x| \leq \sin(\gamma), \\ \frac{1}{\cos(\gamma)}x + \gamma - \tan(\gamma), & \text{if } x > \sin(\gamma). \end{cases}$$

The function \arcsin_γ is continuous and strictly increasing with $\arcsin_\gamma(0) = 0$; its graph for $\gamma = \pi/3$ is shown in Figure 4.1. It is easy to check that \arcsin_γ is a strictly

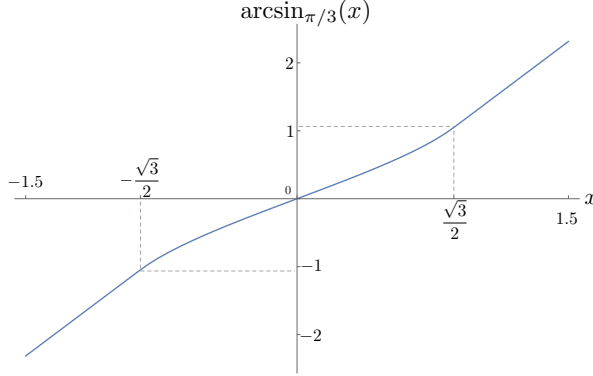


Fig. 4.1: The graph of monotonically increasing function $\arcsin_{\pi/3}$

increasing C^1 -function. For every $\gamma \in [0, \frac{\pi}{2})$ and every $\mathbf{x} = (x_1, \dots, x_n)^\top \in \mathbb{R}^n$, we define $\arcsin_\gamma(\mathbf{x}) = (\arcsin_\gamma(x_1), \dots, \arcsin_\gamma(x_n))^\top$.

Second, recall that given a positive-definite matrix $P \in \mathbb{R}^{m \times m}$, the weighted norm of $x \in \mathbb{R}^m$ is $\|x\|_P^2 = x^\top P x$ and the induced weighted norm of $T \in \mathbb{R}^{m \times m}$ is $\|T\|_P = \|P^{\frac{1}{2}} T P^{-\frac{1}{2}}\|_2$. Note that the diagonal edge weight matrix \mathcal{A} is positive definite.

We are now ready to use the equivalent characterization in Theorem 4.1 to propose an iterative sequence for the active power flow equations (3.2) in a phase-cohesive cell.

THEOREM 4.2 (Projection iteration for solving active power flow equations). *Consider the active power flow equations (3.2) with undirected weighted connected graph G , the incidence matrix B , the Laplacian matrix L , the cutset projection \mathcal{P}_{cut} , the cycle projection \mathcal{P}_{cyc} , cycle basis Σ , and the balanced power supply/demand vector p_{sd} . Given $\gamma \in [0, \frac{\pi}{2})$ and the vector $\mathbf{u} \in \text{Im}g(\mathbf{w}_\Sigma)$, define the projection iteration $\{\eta^{(k)}\}_{k \in \mathbb{Z}_{\geq 0}}$ by $\eta^{(0)} \in \mathbb{R}^m$ and*

$$(4.2) \quad \eta^{(k+1)} = B^\top L^\dagger p_{\text{sd}} + \mathcal{P}_{\text{cyc}} \left(\eta^{(k)} - \cos(\gamma) \left(\arcsin_\gamma(\eta^{(k)}) - 2\pi C_\Sigma^\dagger \mathbf{u} \right) \right).$$

Then the following statements hold:

- (i) there exists a unique fixed point $\eta_{\mathbf{u}}^* \in \mathbb{R}^m$ such that, for every $\eta^{(0)} \in \mathbb{R}^m$, the sequence $\{\eta^{(k)}\}_{k \in \mathbb{Z}_{\geq 0}}$ converges to $\eta_{\mathbf{u}}^*$;
- (ii) for every $\eta^{(0)} \in \mathbb{R}^m$ and every $k \in \mathbb{Z}_{\geq 0}$, we have

$$\|\eta^{(k+1)} - \eta^{(k)}\|_{\mathcal{A}} \leq (1 - \cos(\gamma))^k \|\eta^{(1)} - \eta^{(0)}\|_{\mathcal{A}}.$$

Moreover, the following statements are equivalent:

- (a) we have $\|\eta_{\mathbf{u}}^*\|_{\infty} \leq \sin(\gamma)$;
- (b) the \mathbf{u} -winding edge balance equations (4.1) have a unique solution inside $D_{\infty}(\mathbb{0}_m, \sin(\gamma))$;
- (c) the active power flow equations (3.2) have a unique solution, modulo rotations, inside $\Omega_{\mathbf{u}}^G(\gamma)$.

Finally, if any of the equivalent conditions (a) or (b), or (c) holds, then $\eta_{\mathbf{u}}^*$ is the unique solution for the \mathbf{u} -winding edge balance equations (4.1) and $L^{\dagger}B\mathcal{A}(\arcsin(\eta^*) - 2\pi C_{\Sigma}^{\dagger}\mathbf{u})$ is the unique solution of the active power flow equations (3.2) inside $\Omega_{\mathbf{u}}^G(\gamma)$.

Proof. Regarding parts (i) and (ii), we define the map $H_{\mathbf{u}} : \mathbb{R}^m \rightarrow \mathbb{R}^m$ by

$$H_{\mathbf{u}}(\eta) = B^{\top}L^{\dagger}p_{\text{sd}} + \mathcal{P}_{\text{cyc}}\left(\eta - \cos(\gamma)(\arcsin_{\gamma}(\eta) - 2\pi C_{\Sigma}^{\dagger}\mathbf{u})\right),$$

so that the projection iteration (4.2) can be written $\eta^{(k+1)} = H_{\mathbf{u}}(\eta^k)$. Note that, for every $\eta_1, \eta_2 \in \mathbb{R}^m$,

$$H_{\mathbf{u}}(\eta_1) - H_{\mathbf{u}}(\eta_2) = \mathcal{P}_{\text{cyc}}(\eta_1 - \eta_2 - \cos(\gamma)(\arcsin_{\gamma}(\eta_1) - \arcsin_{\gamma}(\eta_2))).$$

Therefore, by the Mean Value Inequality [1, Proposition 2.4.7],

$$\|H_{\mathbf{u}}(\eta_1) - H_{\mathbf{u}}(\eta_2)\|_{\mathcal{A}} \leq \sup_{x \in \mathbb{R}^m} \|\mathcal{P}_{\text{cyc}}(I_m - \cos(\gamma)\nabla\arcsin_{\gamma}(x))\|_{\mathcal{A}} \|\eta_1 - \eta_2\|_{\mathcal{A}}.$$

Using the fact that $\|\mathbf{x}\|_{\mathcal{A}} = \|\mathcal{A}^{\frac{1}{2}}\mathbf{x}\|_{\mathcal{A}}$, we get

$$\|\mathcal{P}_{\text{cyc}}(I_m - \cos(\gamma)\nabla(\arcsin_{\gamma})(x))\|_{\mathcal{A}} = \left\| \mathcal{A}^{\frac{1}{2}}\mathcal{P}_{\text{cyc}}(I_m - \cos(\gamma)\nabla(\arcsin_{\gamma})(x))\mathcal{A}^{-\frac{1}{2}} \right\|_2.$$

Note that, by triangle inequality, we have

$$\begin{aligned} & \left\| \mathcal{A}^{\frac{1}{2}}\mathcal{P}_{\text{cyc}}(I_m - \cos(\gamma)\nabla(\arcsin_{\gamma})(x))\mathcal{A}^{-\frac{1}{2}} \right\|_2 \\ & \leq \left\| \mathcal{A}^{\frac{1}{2}}\mathcal{P}_{\text{cyc}}\mathcal{A}^{-\frac{1}{2}} \right\|_2 \left\| \mathcal{A}^{\frac{1}{2}}(I_m - \cos(\gamma)\nabla(\arcsin_{\gamma})(x))\mathcal{A}^{-\frac{1}{2}} \right\|_2 \\ & = \left\| \mathcal{A}^{\frac{1}{2}}(I_m - \cos(\gamma)\nabla(\arcsin_{\gamma})(x))\mathcal{A}^{-\frac{1}{2}} \right\|_2, \end{aligned}$$

where in the last inequality we used the fact that $\mathcal{A}^{\frac{1}{2}}\mathcal{P}_{\text{cyc}}\mathcal{A}^{-\frac{1}{2}}$ is a symmetric idempotent matrix and therefore, its 2-norm is equal to 1. Moreover, for every $x \in \mathbb{R}^m$, $\nabla\arcsin_{\gamma}(x)$ is a diagonal matrix such that, for every $i \in \{1, \dots, m\}$, we have

$$(\nabla(\arcsin_{\gamma})(x))_{ii} = \begin{cases} \frac{1}{\sqrt{1-x_i^2}} & \text{if } |x_i| \leq \sin(\gamma), \\ \frac{1}{\cos(\gamma)} & \text{otherwise.} \end{cases}$$

Additionally, by [20, Theorem 5.6.36], we have

$$\begin{aligned} \left\| \mathcal{A}^{\frac{1}{2}}(I_m - \cos(\gamma)\nabla(\arcsin_{\gamma})(x))\mathcal{A}^{-\frac{1}{2}} \right\|_2 &= \|I_m - \cos(\gamma)\nabla(\arcsin_{\gamma})(x)\|_{\infty} \\ &= \max_i \{ |1 - \cos(\gamma)(\nabla(\arcsin_{\gamma})(x))_{ii}| \}. \end{aligned}$$

Note that, for every $x \in \mathbb{R}^m$ and every $i \in \{1, \dots, m\}$, we have

$$|1 - \cos(\gamma)(\nabla(\arcsin_{\gamma})(x))_{ii}| \leq 1 - \cos(\gamma).$$

This implies that

$$\sup_{x \in \mathbb{R}^m} \left\| \mathcal{A}^{\frac{1}{2}} (I_m - \cos(\gamma)) \nabla(\arcsin_\gamma)(x) \mathcal{A}^{-\frac{1}{2}} \right\|_2 = \sup_{x \in \mathbb{R}^m} \|I_m - \cos(\gamma) \nabla(\arcsin_\gamma)(x)\|_\infty \leq 1 - \cos(\gamma).$$

As a result, we get

$$(4.3) \quad \|H_{\mathbf{u}}(\eta_1) - H_{\mathbf{u}}(\eta_2)\|_{\mathcal{A}} \leq (1 - \cos(\gamma)) \|\eta_1 - \eta_2\|_{\mathcal{A}}.$$

Thus, $H_{\mathbf{u}} : \mathbb{R}^m \rightarrow \mathbb{R}^m$ is a contraction mapping with respect to the norm $\|\cdot\|_{\mathcal{A}}$ on the vector space \mathbb{R}^m . Therefore, by the Banach Fixed-point Theorem, there exists a unique $\eta^* \in \mathbb{R}^m$ such that $\eta^* = H_{\mathbf{u}}(\eta^*)$. This completes the proof of part (i).

Regarding part (ii), using the contraction property of $H_{\mathbf{u}}$ (4.3), for every $k \in \mathbb{N}$, we get

$$\|\eta^{(k+1)} - \eta^{(k)}\|_{\mathcal{A}} \leq (1 - \cos(\gamma)) \|\eta^{(k)} - \eta^{(k-1)}\|_{\mathcal{A}}.$$

This implies that, for every $k \in \mathbb{N}$, we have

$$\|\eta^{(k+1)} - \eta^{(k)}\|_{\mathcal{A}} \leq (1 - \cos(\gamma))^k \|\eta^{(1)} - \eta^0\|_{\mathcal{A}}.$$

Now we show the equivalence of the statements (a) and (b).

(a) \implies (b): Since $\eta_{\mathbf{u}}^*$ is the limit point of the converging sequence (4.2), we have

$$\eta_{\mathbf{u}}^* = B^\top L^\dagger p_{\text{sd}} + \mathcal{P}_{\text{cyc}} (\eta_{\mathbf{u}}^* - \cos(\gamma) (\arcsin_\gamma(\eta_{\mathbf{u}}^*) - 2\pi C_\Sigma^\dagger \mathbf{u})).$$

Note that by $\|\eta_{\mathbf{u}}^*\|_\infty \leq \sin(\gamma)$ we get $\arcsin_\gamma(\eta_{\mathbf{u}}^*) = \arcsin(\eta_{\mathbf{u}}^*)$. This implies that

$$(4.4) \quad \eta_{\mathbf{u}}^* = B^\top L^\dagger p_{\text{sd}} + \mathcal{P}_{\text{cyc}} (\eta_{\mathbf{u}}^* - \cos(\gamma) (\arcsin(\eta_{\mathbf{u}}^*) - 2\pi C_\Sigma^\dagger \mathbf{u})).$$

Multiplying both side of equations (4.4) by \mathcal{P}_{cut} and using the fact that $\mathcal{P}_{\text{cut}} \mathcal{P}_{\text{cyc}} = \mathbf{0}_{m \times m}$, we have

$$B^\top L^\dagger p_{\text{sd}} = \mathcal{P}_{\text{cut}} \eta_{\mathbf{u}}^*.$$

Subtracting the above equations from equations (4.4), we get

$$\mathcal{P}_{\text{cyc}} (\arcsin(\eta_{\mathbf{u}}^*) - 2\pi C_\Sigma^\dagger \mathbf{u}) = \mathbf{0}_m.$$

Thus, $\eta_{\mathbf{u}}^*$ satisfies the \mathbf{u} -winding line utilization equations (4.1).

(b) \implies (a): Suppose that $h^* \in D_\infty(0_m, \sin(\gamma))$ is the \mathbf{u} -winding edge balance equations (4.1). Then, we have

$$B^\top L^\dagger p_{\text{sd}} = \mathcal{P}_{\text{cut}} h^* + \cos(\gamma) \mathcal{P}_{\text{cyc}} (\arcsin(h^*) - 2\pi C_\Sigma^\dagger \mathbf{u}).$$

Since $\|h^*\|_\infty \leq \sin(\gamma)$, we have $\arcsin(h^*) = \arcsin_\gamma(h^*)$. Using the fact that $\mathcal{P}_{\text{cyc}} = I_m - \mathcal{P}_{\text{cut}}$, we get

$$h^* = B^\top L^\dagger p_{\text{sd}} - \mathcal{P}_{\text{cyc}} (h^* + \cos(\gamma) (\arcsin(h^*) - 2\pi C_\Sigma^\dagger \mathbf{u})) = H_{\mathbf{u}}(h^*).$$

Thus, $h^* \in D_\infty(0_m, \sin(\gamma))$ is a fixed point of the mapping $H_{\mathbf{u}}$. By part (i), the fixed-point of $H_{\mathbf{u}}$ is unique. Thus, we have $h^* = \eta_{\mathbf{u}}^*$. This implies that $\eta_{\mathbf{u}}^* \in D_\infty(0_m, \sin(\gamma))$. This argument not only shows that (b) implies (a) but also it proves that if one of the

equivalent condition (a) or (b) holds then $\eta_{\mathbf{u}}^*$ is the unique solution of the \mathbf{u} -winding edge balance equations (4.1) inside $D_{\infty}(\mathbb{0}_m, \sin(\gamma))$.

Regarding (b) \iff (c): the proof follows from Theorem 4.1, where the equivalence of the existence of a solution for \mathbf{u} -winding line utilization equations (4.1) with the existence of a solution of the active power flow equations (3.2) inside $\Omega_{\mathbf{u}}^G(\gamma)$ has been established. \square

This theorem establishes that the projection iteration (4.2) correctly computes the solution of the \mathbf{u} -winding edge balance equation (4.1) inside the domain $D_{\infty}(\mathbb{0}_m, \sin(\gamma))$, if one exists. Moreover, the iteration does so with a convergence rate equal to $1 - \cos(\gamma)$; remarkably, this rate is independent of the network size. Naturally, for γ arbitrarily close to $\frac{\pi}{2}$, the convergence rate is arbitrarily low. Finally, assuming each mathematical operation (addition, subtraction, multiplication, and division) is a single floating-point operation (flop), the run-time of the projection iteration (4.2) is $\mathcal{O}(n^3)$ flops. This fact is shown in Appendix B.

As final result in this section, we propose the following algorithm for finding all the solutions of the active power flow equations (3.2) in the phase-cohesive set $\Delta^G(\gamma)$, for some $\gamma \in [0, \frac{\pi}{2})$.

Algorithm 4.1 Active Power Flow Solver

Input: a cyclic connected weighted undirected graph G , a supply/demand vector p_{sd} , and an angle $\gamma \in [0, \frac{\pi}{2})$

Output: all active power flow solution in the γ -phase-cohesive set

- 1: compute a basis $\{\sigma_1, \dots, \sigma_{m-n+1}\}$ for the cycle space of G
 - 2: **for** each candidate winding vector $\mathbf{u} = (w_1, \dots, w_{m-n+1})^\top$ with $w_i \leq \lceil \frac{\gamma n \sigma_i}{2\pi} \rceil$:
 - 3: set $k \leftarrow 0$ and $\eta^{(0)} \leftarrow \mathbb{0}_m$
 - 4: **repeat**
 - 5: $k \leftarrow k + 1$
 - 6: $\eta^{(k)} \leftarrow B^\top L^\dagger p_{\text{sd}} + \mathcal{P}_{\text{cyc}}(\eta^{(k-1)} - \cos(\gamma)(\arcsin_{\gamma}(\eta^{(k-1)}) - 2\pi C_{\Sigma}^\dagger \mathbf{u}))$
 - 7: **until** $\|\eta^{(k)} - \eta^{(k-1)}\|_{\infty} < \text{tolerance}$
 - 8: **if** $\|\eta^{(k)}\|_{\infty} \leq \sin(\gamma)$ **then**
 - 9: **return** $L^\dagger B(\arcsin(\eta^{(k)}) - 2\pi \mathcal{P}_{\text{cyc}} C_{\Sigma}^\dagger \mathbf{u})$ is the solution for (3.2) inside $\Omega_{\mathbf{u}}^G(\gamma)$.
 - 10: **else**
 - 11: **return** there is no solution for (3.2) inside $\Omega_{\mathbf{u}}^G(\gamma)$.
-

COROLLARY 4.3 (A complete solver for active power flow equations). *For every $\gamma \in [0, \frac{\pi}{2})$, the **Active Power Flow Solver** (4.1) finds all solutions of the active power flow equations (3.2) in the phase-cohesive set $\Delta^G(\gamma)$.*

5. Numerical experiments and applications. After developing a solvability theory for the active power flow equations (3.2), we focus on studying the solutions of the active power flow equations using algorithm (4.1). In this section, we consider three simple networks shown in Figure (5.1). Each network is denoted by $\{G, A, p_{\text{sd}}\}$ where G is the underlying graph, A is the edge weight matrix, and $p_{\text{sd}} = P \widehat{p}_{\text{sd}}$ is the balanced supply/demand vector with scaling factor $P > 0$. For every network and every winding number $\mathbf{u} \in \mathbb{Z}$, we define the *power capacity (PC)* of the network as the maximum P for which the active power flow equations (3.2) have a solutions

with winding number \mathbf{u} . Moreover, for every network with a balanced supply/demand vector $p_{\text{sd}} = P\widehat{p}_{\text{sd}}$ and every winding number $\mathbf{u} \in \mathbb{Z}$, we define the maximum network congestion by

$$\max_{(i,j) \in \mathcal{E}} |a_{ij}^{-1} f_{ij}|$$

where $f \in \mathbb{R}^m$ is the solution for the active power flow equations (3.1) with winding number \mathbf{u} .

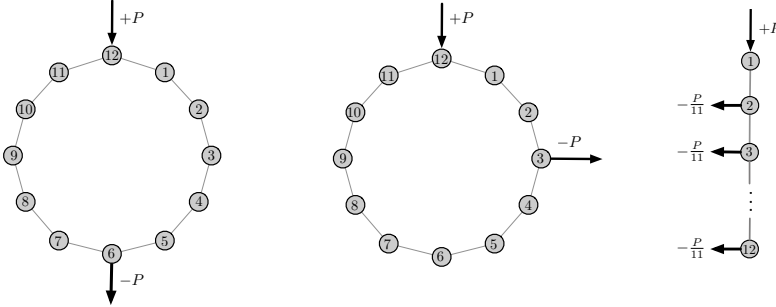


Fig. 5.1: Example networks. Left image: 12-node ring graph with weight matrix $\mathcal{A} = I_{12}$ and symmetric power profile with $p_{\text{sd}} = P[0_5^\top, -1, 0_5^\top, 1]^\top$. Center image: 12-node ring graph with weight matrix $\mathcal{A} = I_{12}$ asymmetric power profile with $p_{\text{sd}} = P[0_2^\top, -1, 0_8^\top, 1]^\top$. Right image: 12-node line graph with weight matrix $\mathcal{A} = I_{11}$ and power profile $p_{\text{sd}} = P[1, -\mathbf{1}_{11}^\top/11]^\top$.

5.1. Symmetric versus asymmetric power injections. In this section, we compare the solutions of the active power flow equations for the networks $\{G, \mathcal{A}, p_{\text{sd}}\}$, with symmetric and asymmetric supply/demand vectors as shown in Figure 5.1. We start from $P = 0$ and increase P by increment of 5×10^{-6} . For each P , we use the algorithm (4.1) with tolerance 10^{-6} to compute the solution of the active power flow equations (3.2). The results of this simulation are shown in Figure 5.2.

Summary evaluation. The winding number 0 does not necessarily carry the maximum PC of a network. As illustrated in Figure 5.2, the winding number -1 carries the largest network PC for the asymmetric supply/demand vector $p_{\text{sd}} = [0_2, -P, 0_8, +P]^\top$. For the asymmetric case, more power can flow along the left path when the winding number is -1 than when the winding number is 0, due to the integer winding number constraint $\mathbf{u} = \frac{1}{2\pi} \mathbf{1}_{12}^\top \arcsin(\mathcal{A}^{-1} f)$. As a result, when the winding number is -1 , the flow along the left path of the ring is able to better relieve the capacity for the right path. \triangle

5.2. Loop flows in IEEE RTS 24 testcase. In this section, we study the loop flows in IEEE RTS 24 testcase. The IEEE RTS 24 is a portion of the larger IEEE RTS 96 testcase which is designed to study reliability of the power networks [18]. This testcase can be described by a connected, undirected graph G with the nodal admittance matrix $Y \in \mathbb{C}^{n \times n}$. The set of nodes are partitioned into load buses \mathcal{V}_1 and generator buses \mathcal{V}_2 . The power demand (resp. power supply) at node $i \in \mathcal{V}_1$ (resp. \mathcal{V}_2) is denoted by the i th element of p_{sd} . The nominal parameters for the test cases can be found in [18] and is shown in the second column of the Table (5.2). We first modify the branches in IEEE RTS 24 to be lossless without shunt admittances. Since our theoretical results assume that all nodes are PV nodes, MATPOWER's solver is

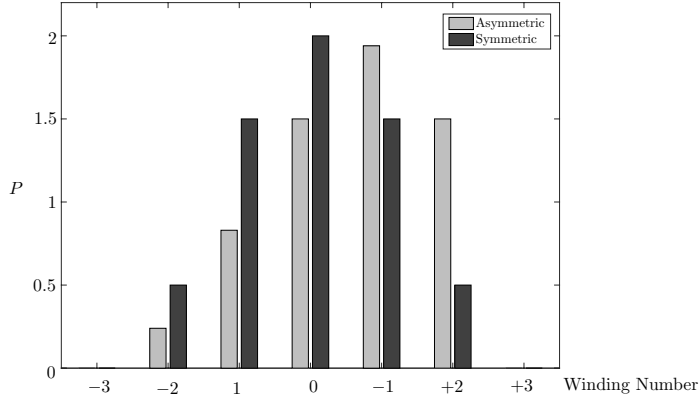


Fig. 5.2: Solutions of active power flow equation with different winding numbers for symmetric and asymmetric graphs shown in Figure 5.1. For the symmetric power profile (left image in Figure 5.1) the largest power capacity is for winding number 0. However, for the asymmetric power profile (middle image in Figure 5.1) the largest power capacity is for winding number -1 .

used to compute the voltage magnitudes at every node [49]. Then the edge weights of G are set to $a_{ij} = a_{ji} = V_i V_j \text{Im}(Y_{ij}) > 0$. Note that the IEEE RTS 24 has 24 buses and 34 branches. Thus, G has a 11-dimensional cycle space of G is an space. A cycle basis for G is $\Sigma = \{\sigma_1, \dots, \sigma_{11}\}$ where, for every $i \in \{1, \dots, 11\}$, the cycle σ_i is given in Table 5.1.

Cycle basis for IEEE RTS 24	
$\sigma_1 = (2, 1, 3, 9, 4, 2)$	$\sigma_2 = (5, 1, 3, 9, 8, 10, 5)$
$\sigma_3 = (10, 6, 2, 4, 9, 8, 10)$	$\sigma_4 = (11, 10, 8, 9, 11)$
$\sigma_5 = (12, 10, 8, 9, 12)$	$\sigma_6 = (13, 11, 9, 12, 23, 13)$
$\sigma_7 = (13, 12, 23, 13)$	$\sigma_8 = (16, 15, 24, 3, 9, 11, 14, 16)$
$\sigma_9 = (21, 15, 24, 3, 9, 11, 14, 16, 17, 22, 21)$	$\sigma_{10} = (21, 18, 17, 22, 21)$
$\sigma_{11} = (23, 20, 19, 16, 14, 11, 9, 12, 23)$	

Table 5.1: A cycle basis Σ for the IEEE RTS 24 testcase

Using the algorithm (4.1), we observe that, for the nominal power supply/demand vector of IEEE RTS 24, there exists no solution of the active power flow equations (3.2) with a nonzero winding vector. Then we modify the power supply/demand vector of the testcase to include a solution with winding vector $\mathbf{u} = [0_{10}^T, -1]$. This supply/demand vector is denoted by p_{sd}^{lp} and is given in the third column of Table 5.2 and the modification in the IEEE RTS 24 testcase is illustrated in Figure 5.3. For the given supply/demand vector p_{sd}^{lp} , there exists exactly one solution associated to the winding vector $\mathbf{u} = 0_{11}$ and one solution associated to the winding vector $\mathbf{u} = [0_{10}^T, -1]$ inside the phase-cohesive set $\Delta^G(1.5)$. The computational time of the projection iteration (4.2) and the MATLAB's *fsolve* for checking the existence/finding these

solutions are compared in Table (5.3).¹

IEEE RTS 24					
Node	p_{sd}^{nom} (MW)	p_{sd}^{lp} (MW)	Node	p_{sd}^{nom} (MW)	p_{sd}^{lp} (MW)
1	64.00	8.40	13	-129.00	-193.50
2	75.00	9.27	14	-194.00	-143.39
3	-180.00	-268.48	15	-102.00	-153.00
4	-74.00	-99.14	16	55.00	00.00
5	-71.00	-79.96	17	00.00	00.00
6	-136.00	-68.63	18	67.00	00.00
7	115.00	63.65	19	-181.00	26.57
8	-171.00	-142.41	20	-128.00	100.00
9	-175.00	-245.21	21	400.00	00.00
10	-195.00	95.83	22	300.00	00.00
11	00.00	100.00	23	660.00	990.00
12	00.00	00.00	24	00.00	00.00

Table 5.2: Nominal supply/demand vector p_{sd}^{nom} versus modified supply/demand vector p_{sd}^{lp} .

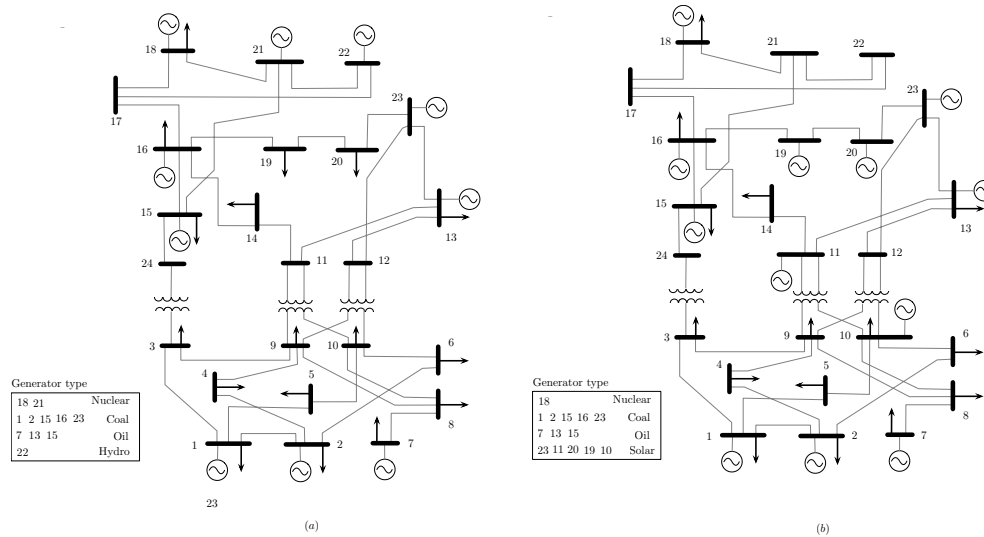


Fig. 5.3: (a) shows the original IEEE RTS 24 test case with generator types and (b) shows the modified IEEE RTS 24 test case. The modifications in power supply/demand vector in Figure (b) are: i) shutting down the hydro generator at node 22 and the nuclear generator at node 21 ii) adding solar energy generations at nodes 10, 11, 19, 20, 23.

Summary evaluation. The ongoing shift from fossil-fueled power generation to renewable energy resources is leading to large changes in the supply/demand structure

¹The computer specifications for these simulations are as follows: Processor Intel Core i5 @ 1.6 GHZ CPU and 4 GB RAM.

Winding vector, \mathbf{u}	$t_{\text{sequence}}/t_{\text{fsolve}}$
$[0_{11}^T]$	0.2463
$[0_{10}^T, -1]$	0.0788

Table 5.3: Computation time for the projection iteration (4.2) for $\gamma = 1.5$ is denoted by t_{sequence} and for MATLAB’s *fsolve* is denoted by t_{fsolve} . The values given in the table are the ratio $t_{\text{sequence}}/t_{\text{fsolve}}$, averaged over 5 trials. The computations use a tolerance of 10^{-6} .

of the power grids. One of the related issues is the change to undesirable operating points, where large powers are flowing over the network. In our simplified model of the power networks, these operating points are associated with the solution of the active power flow equations (3.2) with nonzero winding vector.

- (i) We used the algorithm (4.1) to check for the existence/find all solutions of the active power flow equations (3.2) for IEEE RTS 24 testcase,
- (ii) Table 5.3 shows that, for the IEEE RTS 24 testcase, the projection iteration (4.2) not only converges to the loop flow solutions in the phase cohesive set $\Delta^G(1.5)$ but also is faster than the MATLAB’s *fsolve* for checking the existence/computing the solutions of the active power flow equations.

6. Conclusions. In this paper, we develop a rigorous framework for studying multistable solutions to the active power flow problem. For a graph with phases as nodal variables, we extend Kirchhoff’s voltage law to the n -torus and introduce an equivalence relation that partitions the n -torus into winding cells. Using this partition, we localize stable solutions of the active power flow problem; we show that at most one stable solution exists in each winding cell. In order to check the existence and compute the stable solution in each winding cell, we propose a novel contraction mapping. Finally, we present several numerical experiments to investigate power capacity and congestion in different test cases and check the accuracy and efficiency of our methods.

Much work remains to be done to study the connection of multistability with other phenomena in networks and power systems, such as cluster synchronization and transient stability. First, one of central problem in coupled oscillator networks is characterizing the onset of synchronization [36, 8, 13]. We envision that the winding partition can be utilized to develop analytic necessary and sufficient conditions for synchronization. Second, the treatment in this paper is based on the assumptions of constant voltages and lossless power lines. It is important to investigate multistable power flows in more realistic scenarios, e.g., see [44, 6] for recent work in this direction. Finally, it would be valuable to extend the framework and analysis in this paper to study multistability in general coupled oscillator networks, such as FitzHugh–Nagumo and Hodgkin–Huxley models [11, 33, 17].

REFERENCES

- [1] R. Abraham, J. E. Marsden, and T. S. Ratiu. *Manifolds, Tensor Analysis, and Applications*, volume 75 of *Applied Mathematical Sciences*. Springer, 2 edition, 1988.
- [2] J. A. Acebrón, L. L. Bonilla, C. J. P. Vicente, F. Ritort, and R. Spigler. The Kuramoto model: A simple paradigm for synchronization phenomena. *Reviews of Modern Physics*, 77(1):137–185, 2005. doi:10.1103/RevModPhys.77.137.
- [3] P. M. Anderson and A. A. Fouad. *Power System Control and Stability*. John Wiley & Sons, 2 edition, 2002.

- [4] A. Arenas, A. Díaz-Guilera, J. Kurths, Y. Moreno, and C. Zhou. Synchronization in complex networks. *Physics Reports*, 469(3):93–153, 2008. doi:10.1016/j.physrep.2008.09.002.
- [5] A. R. Bergen and D. J. Hill. A structure preserving model for power system stability analysis. *IEEE Transactions on Power Apparatus and Systems*, 100(1):25–35, 1981. doi:10.1109/TPAS.1981.316883.
- [6] J. C. Bronski, T. Carty, and L. DeVille. Configurational stability for the Kuramoto–Sakaguchi model. *Chaos: An Interdisciplinary Journal of Nonlinear Science*, 28(10):103109, 2018. doi:10.1063/1.5029397.
- [7] F. Bullo. *Lectures on Network Systems*. Kindle Direct Publishing, 1.3 edition, July 2019. With contributions by J. Cortés, F. Dörfler, and S. Martínez. URL: <http://motion.me.ucsb.edu/book-Ins>.
- [8] N. Chopra and M. W. Spong. On exponential synchronization of Kuramoto oscillators. *IEEE Transactions on Automatic Control*, 54(2):353–357, 2009. doi:10.1109/TAC.2008.2007884.
- [9] T. Coletta, R. Delabays, I. Adagideli, and P. Jacquod. Topologically protected loop flows in high voltage AC power grids. *New Journal of Physics*, 18(10):103042, 2016. doi:10.1088/1367-2630/18/10/103042.
- [10] R. Delabays, T. Coletta, and P. Jacquod. Multistability of phase-locking and topological winding numbers in locally coupled Kuramoto models on single-loop networks. *Journal of Mathematical Physics*, 57(3):032701, 2016. doi:10.1063/1.4943296.
- [11] M. Desroches, J. Guckenheimer, B. Krauskopf, C. Kuehn, H. Osinga, and M. Wechselberger. Mixed-mode oscillations with multiple time scales. *SIAM Review*, 54(2):211–288, 2012. doi:10.1137/100791233.
- [12] F. Dörfler and F. Bullo. Synchronization in complex networks of phase oscillators: A survey. *Automatica*, 50(6):1539–1564, 2014. doi:10.1016/j.automatica.2014.04.012.
- [13] F. Dörfler, M. Chertkov, and F. Bullo. Synchronization in complex oscillator networks and smart grids. *Proceedings of the National Academy of Sciences*, 110(6):2005–2010, 2013. doi:10.1073/pnas.1212134110.
- [14] M. Elkin, C. Liebchen, and R. Rizzi. New length bounds for cycle bases. *Information Processing Letters*, 104(5):186–193, 2007. doi:10.1016/j.ipl.2007.06.013.
- [15] G. B. Ermentrout. The behavior of rings of coupled oscillators. *Journal of Mathematical Biology*, 23(1):55–74, 1985. doi:10.1007/BF00276558.
- [16] T. Ferguson. Topological states in the Kuramoto model. *SIAM Journal on Applied Dynamical Systems*, 17(1):484–499, 2018. doi:10.1137/17M112484X.
- [17] A. Franci, G. Drion, and R. Sepulchre. Modeling the modulation of neuronal bursting: A singularity theory approach. *SIAM Journal on Applied Dynamical Systems*, 13(2):798–829, 2014. doi:10.1137/13092263X.
- [18] C. Grigg et al. The IEEE Reliability Test System-1996. A report prepared by the Reliability Test System Task Force of the Application of Probability Methods Subcommittee. *IEEE Transactions on Power Systems*, 14(3):1010–1020, 1999. doi:10.1109/59.780914.
- [19] NERC Steering Group. Technical Analysis of the August 14, 2003, Blackout: What Happened, Why, and What Did We Learn? Technical report, North American Electric Reliability Council, Princeton Forrestal Village, Princeton, NJ, USA, July 2004.
- [20] R. A. Horn and C. R. Johnson. *Matrix Analysis*. Cambridge University Press, 2nd edition, 2012.
- [21] J. D. Horton. A polynomial-time algorithm to find the shortest cycle basis of a graph. *SIAM Journal on Computing*, 16(2):358–366, 1987. doi:10.1137/0216026.
- [22] S. Jafarpour and F. Bullo. Synchronization of Kuramoto oscillators via cutset projections. *IEEE Transactions on Automatic Control*, 64(7):2830–2844, 2019. doi:10.1109/TAC.2018.2876786.
- [23] N. Janssens and A. Kamagate. Loop flows in a ring AC power system. *International Journal of Electrical Power & Energy Systems*, 25(8):591–597, 2003. doi:10.1016/S0142-0615(03)00017-6.
- [24] T. Kavitha, C. Liebchen, K. Mehlhorn, D. Michail, R. Rizzi, T. Ueckerdt, and K. A. Zweig. Cycle bases in graphs characterization, algorithms, complexity, and applications. *Computer Science Review*, 3(4):199–243, 2009. doi:10.1016/j.cosrev.2009.08.001.
- [25] A. J. Kersak. On the question of uniqueness of stable load-flow solutions. *IEEE Transactions on Power Apparatus and Systems*, 91(3):1093–1100, 1972. doi:10.1109/TPAS.1972.293463.
- [26] P. Kundur. *Power System Stability and Control*. McGraw-Hill, 1994.
- [27] F. Lazebnik. On systems of linear Diophantine equations. *Mathematics Magazine*, 69(4):261–266, 1996. doi:10.2307/2690528.
- [28] B. Lesieutre and D. Wu. An efficient method to locate all the load flow solutions - revisited. In

- Allerton Conf. on Communications, Control and Computing*, pages 381–388, Monticello, IL, USA, October 2015. doi:10.1109/ALLERTON.2015.7447029.
- [29] S. H. Low. Convex relaxation of optimal power flow — Part I: Formulations and equivalence. *IEEE Transactions on Control of Network Systems*, 1(1):15–27, 2014. doi:10.1109/TCNS.2014.2309732.
- [30] W. Ma and J. S. Thorp. An efficient algorithm to locate all the load flow solutions. *IEEE Transactions on Power Systems*, 8(3):1077–1083, 1993. doi:10.1109/59.260891.
- [31] D. Manik, M. Timme, and D. Witthaut. Cycle flows and multistability in oscillatory networks. *Chaos: An Interdisciplinary Journal of Nonlinear Science*, 27(8):083123, 2017. doi:10.1063/1.4994177.
- [32] G. S. Medvedev. Small-world networks of Kuramoto oscillators. *Physica D: Nonlinear Phenomena*, 266:13–22, 2014. doi:10.1016/j.physd.2013.09.008.
- [33] G. S. Medvedev and N. Kopell. Synchronization and transient dynamics in the chains of electrically coupled Fitzhugh-Nagumo oscillators. *SIAM Journal on Applied Mathematics*, 61(5):1762–1801, 2001. doi:10.1137/S0036139900368807.
- [34] G. S. Medvedev and X. Tang. Stability of twisted states in the Kuramoto model on Cayley and random graphs. *Journal of Nonlinear Science*, 25(6):1169–1208, 2015. doi:10.1007/s00332-015-9252-y.
- [35] D. Mehta, N. S. Daleo, F. Dörfler, and J. D. Hauenstein. Algebraic geometrization of the Kuramoto model: Equilibria and stability analysis. *Chaos: An Interdisciplinary Journal of Nonlinear Science*, 25(5):053103, 2015. doi:10.1063/1.4919696.
- [36] R. E. Mirolo and S. H. Strogatz. The spectrum of the locked state for the Kuramoto model of coupled oscillators. *Physica D: Nonlinear Phenomena*, 205(1-4):249–266, 2005. doi:10.1016/j.physd.2005.01.017.
- [37] D. K. Molzahn, F. Dörfler, H. Sandberg, S. H. Low, S. Chakrabarti, R. Baldick, and J. Lavaei. A survey of distributed optimization and control algorithms for electric power systems. *IEEE Transactions on Smart Grid*, 8(6):2941–2962, 2017. doi:10.1109/TSG.2017.2720471.
- [38] D. K. Molzahn, B. C. Lesieutre, and H. Chen. Counterexample to a continuation-based algorithm for finding all power flow solutions. *IEEE Transactions on Power Systems*, 28(1):564–565, 2013. doi:10.1109/TPWRS.2012.2202205.
- [39] J. A. Momoh, R. Adapa, and M. E. El-Hawary. A review of selected optimal power flow literature to 1993. I. Nonlinear and quadratic programming approaches. *IEEE Transactions on Power Systems*, 14(1):96–104, 1999. doi:10.1109/59.744492.
- [40] J. A. Momoh, M. E. El-Hawary, and R. Adapa. A review of selected optimal power flow literature to 1993. II. Newton, linear programming and interior point methods. *IEEE Transactions on Power Systems*, 14(1):105–111, 1999. doi:10.1109/59.744495.
- [41] M. A. Porter and J. P. Gleeson. *Dynamical Systems on Networks: A Tutorial*. Springer, 2016. doi:10.1007/978-3-319-26641-1.
- [42] S. Rao, Y. Feng, D. J. Tylavsky, and J. K. Subramanian. The holomorphic embedding method applied to the power-flow problem. *IEEE Transactions on Power Systems*, 31(5):3816–3828, 2016. doi:10.1109/TPWRS.2015.2503423.
- [43] J. A. Rogge and D. Aeyels. Stability of phase locking in a ring of unidirectionally coupled oscillators. *Journal of Physics A: Mathematical and General*, 37(46):11135–11148, 2004. doi:10.1088/0305-4470/37/46/004.
- [44] J. W. Simpson-Porco. A theory of solvability for lossless power flow equations – Part I: Fixed-point power flow. *IEEE Transactions on Control of Network Systems*, 5(3):1361–1372, 2018. doi:10.1109/TCNS.2017.2711433.
- [45] Lake Erie Loop Flow Mitigation. Technical report, New York Independent System Operator, November 2008. URL: <https://studylib.net/doc/18746699/lake-erie-loop-flow-mitigation>.
- [46] A. Trias. The holomorphic embedding load flow method. In *IEEE Power & Energy Society General Meeting*, pages 1–8, 2012. doi:10.1109/PESGM.2012.6344759.
- [47] United States Department of Energy. Transmission Constraints and Congestion in the Western and Eastern Interconnections, 2009–2012. Technical report, Washington, DC, USA, January 2014. URL: <https://www.energy.gov/oe/downloads/transmission-constraints-and-congestion-western-and-eastern-interconnections-2009-2012>.
- [48] D. A. Wiley, S. H. Strogatz, and M. Girvan. The size of the sync basin. *Chaos: An Interdisciplinary Journal of Nonlinear Science*, 16(1):015103, 2006. doi:10.1063/1.2165594.
- [49] R. D. Zimmerman, C. E. Murillo-Sánchez, and R. J. Thomas. MATPOWER: Steady-state operations, planning, and analysis tools for power systems research and education. *IEEE Transactions on Power Systems*, 26(1):12–19, 2011. doi:10.1109/TPWRS.2010.2051168.

Appendix A. A useful lemma.

LEMMA A.1 (Properties of the cycle-edge matrix). *Given a cyclic connected undirected graph G with cycle basis $\Sigma = \{\sigma_1, \dots, \sigma_{m-n+1}\}$, the following statements hold:*

- (i) *the matrix C_Σ is of rank $m - n + 1$,*
- (ii) *$\text{Ker}(C_\Sigma) = \text{Img}(B^\top)$,*
- (iii) *the system of equations $C_\Sigma \mathbf{z} = \mathbf{v}$, for $\mathbf{v} \in \text{Img}(\mathbf{w}_\Sigma)$, has an integer solution.*

Proof. Regarding part (i), note that rank of the matrix C_Σ is equal to the number of linearly independent rows in C_Σ . By definition, the set $\{\sigma_1, \dots, \sigma_{m-n+1}\}$ consists of linearly independent vectors in \mathbb{R}^m and thus rank of C_Σ is equal to $m - n + 1$.

Regarding part (ii), we first show that $\text{Img}(B^\top) \subseteq \text{Ker}(C_\Sigma)$. Suppose that $\mathbf{y} \in \text{Img}(B^\top)$. Then there exists $\mathbf{x} \in \mathbb{R}^n$ such that $\mathbf{y} = B^\top \mathbf{x}$. Thus, for every $i \in \{1, \dots, m - n + 1\}$, we get

$$v_{\sigma_i}^\top \mathbf{y} = v_{\sigma_i}^\top B^\top \mathbf{x} = (B v_{\sigma_i})^\top \mathbf{x} = 0,$$

where the last equality holds since $v_\sigma \in \text{Ker}(B)$, for every cycle σ . This means that $C_\Sigma \mathbf{y} = 0$ or equivalently $\mathbf{y} \in \text{Ker}(C_\Sigma)$. Therefore, $\text{Img}(B^\top) \subseteq \text{Ker}(C_\Sigma)$. In turn, using the result in part (i), rank of the matrix C_Σ is $m - n + 1$. Thus, by the rank-nullity theorem, we have

$$\dim(\text{Ker}(C_\Sigma)) = m - (m - n + 1) = n - 1 = \dim(\text{Img}(B^\top)).$$

As a result, we have $\text{Img}(B^\top) = \text{Ker}(C_\Sigma)$.

Regarding part (iii), suppose that Σ' is an integral cycle basis for G (for a definition and existence of an integral cycle basis see [24]). Since Σ is a cycle basis for G , there exists an invertible integer matrix $T \in \mathbb{R}^{(m-n+1) \times (m-n+1)}$ such that

$$v_{\sigma'_i} = \sum_{j=1}^n t_{ji} v_{\sigma_j}.$$

This implies that $C_{\Sigma'} = T C_\Sigma$. We first show that the system of linear equations $C_{\Sigma'} \mathbf{z} = T \mathbf{u}$ has an integer solution. Note that rank of the matrix $C_{\Sigma'}$ is $m - n + 1$. Let \mathcal{T} be a spanning tree in G and without loss of generality, assume that the first $m - n + 1$ column of $C_{\Sigma'}$ are associated with the edges that are not in the spanning tree \mathcal{T} . Then, we define the matrix $\widehat{C}_{\Sigma'} \in \mathbb{R}^{(m-n+1) \times (m-n+1)}$ as follows:

$$\widehat{C}_{\Sigma'} = [(C_{\Sigma'})_1 \quad \dots \quad (C_{\Sigma'})_{m-n+1}].$$

where $(C_{\Sigma'})_i$ the i th column of the matrix $C_{\Sigma'}$. Since Σ' is an integral base, by [24, Theorem 3.4], we have $|\det(\widehat{C}_{\Sigma'})| = 1$. Since the matrix $\widehat{C}_{\Sigma'}$ has integer entries, by [27, Theorem 1], there exists matrices $U, V \in \mathbb{Z}^{(m-n+1) \times (m-n+1)}$ with $|\det(U)| = |\det(V)| = 1$ such that

$$U \widehat{C}_{\Sigma'} V = B = \text{diag}(b_1, \dots, b_{m-n+1}),$$

where b_i are positive integers and $b_i | b_{i+1}$, for every $i \in \{1, \dots, m - n\}$. Note that $|\det(\widehat{C}_{\Sigma'})| = 1$ implies that $|\det(B)| = 1$ which in turn implies that $|b_i| = 1$, for every $i \in \{1, \dots, m - n + 1\}$. Therefore, by [27, Proposition 2], for every $\mathbf{v} \in \mathbb{Z}^{(m-n+1)}$, there exists an integer solution $\mathbf{x} \in \mathbb{Z}^{(m-n+1)}$ such that $\widehat{C}_{\Sigma'}(\mathbf{x}) = T \mathbf{u}$. Then it is straightforward to see that the integer vector $\mathbf{z} \in \mathbb{Z}^m$ defined by

$$\mathbf{z} = \begin{bmatrix} \mathbf{x} \\ \mathbf{0}_{n-1} \end{bmatrix}$$

is a solution for the system of equations $C_{\Sigma'}\mathbf{z} = T\mathbf{u}$. This means that $TC_{\Sigma}\mathbf{z} = T\mathbf{u}$ and since T is invertible, we have $C_{\Sigma}\mathbf{z} = \mathbf{u}$. This completes the proof of Lemma A.1. \square

Appendix B. Computational complexity of the projection iteration.

In this appendix, we study the computational complexity of the projection iteration (4.2) for checking the existence/computing the solutions of active power flow equations in each winding cells. As a first step, we prove the following useful lemma.

LEMMA B.1. *Consider an undirected weighted connected graph G with a cycle basis Σ . Then, for every $\mathbf{u} \in \text{Img}(\mathbf{w}_{\Sigma})$, the system of linear equations*

$$(B.1) \quad C_{\Sigma}\mathbf{z} = \mathbf{u},$$

can be solved in $\mathcal{O}(nm)$.

Proof. Let \mathcal{T} be a spanning tree in G and, without loss of generality, assume that $\mathcal{E} - \mathcal{E}_{\mathcal{T}} = \{e_1, \dots, e_{m-n+1}\}$. Then, for every $i \in \{1, \dots, m-n+1\}$, we define the cycle σ'_i as follows:

$$\sigma'_i = (i_1, \dots, i_k, i_1),$$

where $e_i = (i_1, i_k)$ and (i_1, \dots, i_k) is the unique simple path in the spanning tree \mathcal{T} between nodes i_1 and i_k . Then one can easily show that $\Sigma' = \{\sigma'_1, \dots, \sigma'_{m-n+1}\}$ is a cycle basis for G . Since Σ is also a cycle basis for G , there exists an invertible matrix $R = \{r_{ij}\}$ such that

$$(B.2) \quad v_{\sigma'_i} = \sum_{j=1}^{m-n+1} r_{ji} v_{\sigma_j}$$

Moreover, each cycle in G has at most n edges, it is easy to check that, at most n entries in each rows of R are non-zero. Using equations (B.2), one can deduce that $C_{\Sigma'} = RC_{\Sigma}$. This implies that \mathbf{z} is a solution for equations (B.1) if and only if it is a solution for $C_{\Sigma'}\mathbf{z} = R\mathbf{u}$. Note that $\mathbf{z} = [\mathbf{0}_{n-1}, R\mathbf{u}]^{\top}$ is a solution to $C_{\Sigma'}\mathbf{z} = R\mathbf{u}$ and therefore a solution to equations (B.1). Thus, by computing $R\mathbf{u}$, one can find the solution to the linear systems of equations (B.1). Note $R \in \mathbb{R}^{(m-n+1) \times (m-n+1)}$ and in each row of R there is at most n non-zero element. Thus, the computational complexity of finding $R\mathbf{u}$ and finding a solution for (B.1) is $\mathcal{O}(nm)$. \square

Now we can prove the main result of this appendix.

THEOREM B.2 (Computational complexity of the projection iteration (4.2)). *Consider the active power flow equations (3.2) with undirected weighted connected graph G , the incidence matrix B , the Laplacian matrix L , the cutset projection \mathcal{P}_{cut} , the cycle projection \mathcal{P}_{cyc} , cycle basis Σ , and the power injections p_{sd} . Given $\gamma \in [0, \frac{\pi}{2})$ and the vector $\mathbf{u} \in \text{Img}(\mathbf{w}_{\Sigma})$, the computational complexity of the projection iteration (4.2) to check for the existence and/or compute the solution of the active power flow equations (3.2) in the winding cell $\Omega_{\mathbf{u}}^G(\gamma)$ is $\mathcal{O}(n^3)$ in time.*

Proof. The computational time of the iterations (3.2) to check for the existence and/or compute the solution of the active power flow equations (3.2) is

$$(B.3) \quad (\text{Computational time for each iterations}) \times (\text{the number of iterations}).$$

The number of iterations is bounded above by

$$\frac{\log(\mathcal{E}) - \log(\|B^{\top}L^{\dagger}p_{\text{sd}} + 2\cos(\gamma)\pi\mathcal{P}_{\text{cyc}}C_{\Sigma}^{\dagger}\mathbf{u}\|_{\mathcal{A}})}{\log(1 - \cos(\gamma))},$$

which is independent of n and m . Therefore, the number of iterations is $\mathcal{O}(1)$. For each iteration step, we need to compute the terms i) $B^\top L^\dagger p_{\text{sd}}$, ii) $\mathcal{P}_{\text{cyc}} \eta^{(k)}$, iii) $\cos(\gamma) \mathcal{P}_{\text{cyc}} \arcsin_\gamma(\eta^{(k)})$, and iv) $2\pi \mathcal{P}_{\text{cyc}} C_\Sigma^\dagger \mathbf{u}$ and then add them together.

- (i) This term can be written as $B^\top(L^\dagger p_{\text{sd}}) = B^\top \mathbf{x}$, where \mathbf{x} is the solution of the following linear system of equations

$$(B.4) \quad L\mathbf{x} = p_{\text{sd}}.$$

Using the LU decomposition method, one can compute \mathbf{x} in $\mathcal{O}(n^3)$. Moreover, since each row in matrix B^\top has exactly 2 nonzero element, given \mathbf{x} , the $B^\top(L^\dagger p_{\text{sd}}) = B^\top \mathbf{x}$ can be computed in $\mathcal{O}(n)$. Therefore, the computational time for computing the term $B^\top L^\dagger p_{\text{sd}}$ is in $\mathcal{O}(n^3)$.

- (ii) For this term $\mathcal{P}_{\text{cyc}} \eta^{(k)}$, note that $\mathcal{P}_{\text{cyc}} \eta^{(k)} = (I_m - B^\top L^\dagger B A) \eta^{(k)} = \eta^{(k)} - B^\top L^\dagger B A \eta^{(k)}$. The term $B^\top L^\dagger B A \eta^{(k)} = B^\top \mathbf{y}$, where \mathbf{y} is the solution to the linear equations

$$L\mathbf{y} = B A \eta^{(k)}.$$

Using a similar argument, one can show that $B^\top L^\dagger B A \eta^{(k)} = B^\top \mathbf{y}$ can be computed in $\mathcal{O}(n^3)$ and therefore $\mathcal{P}_{\text{cyc}} \eta^{(k)}$ can be computed in $\mathcal{O}(n^3)$.

- (iii) Since $\arcsin_\gamma(\eta^{(k)}) \in \mathbb{R}^m$, it can be computed in $\mathcal{O}(m)$. Then, the term $\cos(\gamma) \mathcal{P}_{\text{cyc}} \arcsin_\gamma(\eta^{(k)})$ can be computed in $\mathcal{O}(n^3)$.
- (iv) Since $\text{Ker}(C_\Sigma) = \text{Img}(B^\top) = \text{Ker}(\mathcal{P}_{\text{cyc}})$, then we have $2\pi \mathcal{P}_{\text{cyc}} C_\Sigma^\dagger \mathbf{u} = 2\pi \mathcal{P}_{\text{cyc}} \mathbf{z}$, where \mathbf{z} is the solution of the following linear system of equations

$$C_\Sigma \mathbf{z} = \mathbf{u}.$$

By Lemma B.1, \mathbf{z} can be computed in $\mathcal{O}(mn)$. This implies that

$$2\pi \mathcal{P}_{\text{cyc}} C_\Sigma^\dagger \mathbf{u} = 2\pi \mathcal{P}_{\text{cyc}} \mathbf{z}$$

can be computed in $\mathcal{O}(n^3)$. \square

Therefore, each step for the projection iteration can be computed in $\mathcal{O}(n^3)$ and, by equation (B.3), the projection iteration (4.2) can done in $\mathcal{O}(n^3) \times \mathcal{O}(1) = \mathcal{O}(n^3)$ time.